ADVANCED FUNCTIONAL MATERIALS

Supporting Information

for *Adv. Funct. Mater.*, DOI: 10.1002/adfm.201809112

Sequence-Optimized Peptide Nanofibers as Growth Stimulators for Regeneration of Peripheral Neurons

Corinna Schilling, Thomas Mack, Selene Lickfett, Stefanie Sieste, Francesco S. Ruggeri, Tomas Sneideris, Arghya Dutta, Tristan Bereau, Ramin Naraghi, Daniela Sinske, Tuomas P. J. Knowles, Christopher V. Synatschke, Tanja Weil, and Bernd Knöll**

Sequence-Optimized Peptide Nanofibers as Growth Stimulators for Regeneration of Peripheral Neurons

Corinna Schilling[1,#], Thomas Mack[2,4 #,] Selene Lickfett[1], Stefanie Sieste[2,4], Francesco S. Ruggeri[3], Tomas Sneideris[3] Arghya Dutta[4], Tristan Bereau[4], Ramin Naraghi[5], Daniela Sinske[1], Tuomas P. J. Knowles[3], Christopher V. Synatschke[6], Tanja Weil[2, 6, *], Bernd Knöll[1,*]

[1] Institute of Physiological Chemistry
Ulm University
Albert-Einstein-Allee 11
89081 Ulm
Germany

[2] Institute of Inorganic Chemistry I
Ulm University
Albert-Einstein-Allee 11
89081 Ulm
Germany

[3] Department of Chemistry
University of Cambridge
Cambridge CB2 1EW
UK

[4] Max Planck Institute for Polymer Research
Ackermannweg 10
55128 Mainz
Germany

[5] Department of Neurosurgery
German Armed Forces Hospital Ulm
Oberer Eselsberg 40
89081 Ulm
Germany

[6] Department Synthesis of Macromolecules
Max Planck Institute for Polymer Research
Ackermannweg 10
55128 Mainz

*co-corresponding authors
# both authors contributed equally

Supplementary Materials & methods

Materials for peptide synthesis and characterization

PyBOP, Fmoc-Lys(Boc)-OH, Fmoc-Phe-OH, Fmoc-Gln(Trt)-OH, Fmoc-Ile-OH, Fmoc-Cys(Trt)-OH, Fmoc-Arg(Pbf)-OH, Fmoc-Gly-OH, Fmoc-Asp(OtBu)-OH, Fmoc-Trp(Boc)-OH, Fmoc-Asn(Trt)-OH, Fmoc-Met-OH, Fmoc-Leu-OH, Fmoc-Phe-Wang resin, Fmoc-Ile-Wang resin, Fmoc-Gln(Trt)-Wang resin, Fmoc-Asp(OtBu)-Wang resin, Fmoc-Trp(Boc)-Wang resin, Fmoc-Leu-Wang resin, Fmoc-Met-Wang resin and Fmoc-Cys(Trt)-Wang resin were purchased from Novabiochem®. N-ethyldiisopropylamine for synthesis (DIPEA), potassium chloride (KCl) and rhodamine B isothiocyanate (RITC) were obtained from Merck. Piperidine (≥ 99.5 % for peptide synthesis) and trifluoroacetic acid (TFA, ≥ 99.9 %) were obtained from Carl Roth. Dimethylformamide (DMF, peptide synthesis), diethyl ether and acetonitrile (HiPerSolv Chromanorm for HPLC-gradient grade) were purchased from VWR Chemicals Prolabo. Dimethylsulfoxid (DMSO, ACS reagent, ≥ 99.9 %) was purchased from Honeywell, Riedel-de Haën®. Vivaspin 500 tubes (3 kDa MWCO) were purchased from Sartorius. Syringe filters Chromafil®Xtra RC-20/13 (0.20 µm) were obtained from Machery-Nagel. Uranyl acetate was purchased from Merck. Fluorescamine was purchased from PanReac AppliChem. Proteinase K and α-Cyano-4-hydroxycinnamic acid were purchased from Sigma Aldrich. The peptide SAP[8a] was purchased from Cassie Peptides, China.

Methods

Solid-phase peptide synthesis

All peptides were synthesized according to standard microwave-assisted Fmoc solid-phase peptide synthesis with amino acid pre-loaded Wang resins from the *C* to *N*

terminus on a 0.1 mM scale. Fmoc-deprotection was carried out with dimethylformamide (DMF) solutions containing 20% to 25% (v/v) piperidine. Coupling reactions were done with 5 eq of amino acid catalyzed by 5 eq hexafluorophosphate benzotriazole tetramethyl uronium (HBTU) or benzotriazol-1-yl-oxytripyrrolidinophosphonium hexafluorophosphate (PyBOP) and 10 eq *N,N*-diisopropylethylamine (DIPEA). Cleavage from the resin and side chain deprotection was carried out by addition of a mixture of trifluoroacetic acid (TFA), triisopropylsilane (TIS) and H_2O at a ratio of 95:2.5:2.5 by shaking at RT for 2 h. Cleaved peptides were precipitated in cold diethylether and lyophilized.

Purification of SAPs

All peptides were purified via HPLC using a binary gradient with an eluant mixture of 0.1 % TFA water-acetonitrile. For preparative scale a Shimadzu system was used (LC-20AP, CBM-20A, SPD-20A) with a reversed phase C18 column (LiChrospher, Merck). Analytical scale was performed onto an analytical ChroCART® 125-4 column (LiChrospher, Merck) with a 1260 Infinity Quarternary LC System (Agilent Technologies). All peptides were analyzed by matrix assisted laser desorption/ionization time of flight (MALDI-TOF, Bruker Reflex III) using 4-Hydroxy-α-cyanocinnaminic acid as matrix.

SAP fiber formation

Lyophilized peptide was dissolved in DMSO to yield a 10 mg/mL stock solution, which was stored at 4 °C prior to usage. The stock solution was diluted tenfold in freshly filtered PBS or ddH_2O (0.22 µm pore size) to initiate fiber formation. All peptides were incubated at a final concentration of 1 mg/mL for at least 16 h to

ensure complete fiber formation at room temperature. Lower concentrations indicated in the text were achieved by dilution of preformed fibers.

Transmission electron microscopy (TEM)

5 µL of each SAP were deposited on copper grids, which were coated with a thin electron-transparent Formvar-layer and were freshly etched with oxygen plasma before use. After 5 min incubation time, excess sample solution was removed with filter paper and the copper grid was further incubated for 5 minutes in 2% uranyl acetate solution to enhance sample contrast. After staining, the samples were washed three times in MilliQ-water, dried in air and micrographs were taken in high vacuum with an EM 109 transmission electron microscope (Zeiss) at an acceleration voltage of 80 kV. Pictures were processed with the EM109 microscope software ImageSP V1.2.6.22.

Atomic Force Microscopy (AFM)

AFM samples were prepared on the freshly functionalized MICA surfaces by the deposition of a 10 µL drop of protein (2 µM) for 5 min. Salts were washed away with 1 ml of MilliQ water and the samples were stored in sealed containers until imaging.

High-resolution images (1024x1024 pixels) were collected using an NX10 Atomic Force Microscopy (Park Systems, South Korea) in ambient conditions and in non-contact Amplitude Modulation (NC-AM). We performed all the measurements using sharp cantilevers (PPP-NCHR, Park Systems, South Korea) with resonance frequency of 330 kHz and typical radius of curvature of 8 nm. Raw images were flattened with the XEI software (Park System, South Korea). In order to keep consistency in the further statistical analysis, all images were processed with the same parameters. Cross-sectional height of individual fibrillar aggregates was

quantified as the maximum of the cross-sectional profile perpendicular to the main axis of symmetry of the fibril, by using SPIP (Image metrology, Denmark) software. Data were analyzed and histograms were created using OriginPro (OriginLab) software.

Zeta potential

The electrophoretic mobility of fibrils was measured to enable comparisons of surface charge. 50 µL of preformed fibrils were diluted in 950 µL of 1 mM freshly prepared and filtered (pore size 0.22 µm) KCl solution. The sample solutions were measured in 1 mL disposable folded capillary cells (Zetasizer Nano series, Malvern) on a Zetasizer Nano ZS (Malvern Instruments) at ambient temperature. The mobility was converted to corresponding ζ-potential values by processing the data with the Zetasizer Nano ZS Software (V7.12). The ζ-potential was calculated by the mean value achieved of at least three independent measurements à 20 runs.

Proteostat® Assay

Fluorescence spectra were recorded on an Infinite® M1000 PRO microplate reader (Tecan). 9 µL of sample aliquots were placed in black UV Star® 384 microliter well-plates (Greiner bio-one). A ProteoStat® solution was prepared according to manufacturers' protocol and diluted hundred-fold in PBS. After addition of 1 µL of Proteostat® solution to all samples and 10 min incubation time, the fluorescence emission was recorded at 603 nm upon excitation at 550 nm with multiple reads per well (3x3).

Conversion rate assay

To determine the amount of peptide monomer converting into fibers we established a fluorescence-based assay. Each peptide sample was incubated as previously described (200 µL). 100 µL per sample was centrifuged in a Vivaspin 500 tube (3kDa MWCO) to separate fibers from free peptide monomer (13 krpm, 4°C, 45 min). The filtrate and the other 100 µL of sample (original sample) were lyophilized and dissolved in 25 µL DMSO to suppress fiber formation. The amount of peptide was determined by adding the amine reactive dye fluorescamine and measuring fluorescence enhancement. In a black 384-well-plate (Greiner Bio-one) 10 µL of the DMSO samples (filtrate and original sample) were submitted and 3 µL of fluorescamine solution (10 mg/mL, DMSO) was added. After 20 min of incubation at RT, fluorescence was measured with an excitation wavelength of λ_{ex} = 365 nm and an emission wavelength of λ_{em} = 470 nm with multiple reads 3x3 (Infinite® M1000 PRO microplate reader). All values were calculated as n-fold fluorescence enhancement (DMSO only as a reference was set to 1). The conversion rate CR was defined according to the following equation:

$$CR = 100 - \frac{100 \cdot \text{Fluorescence Intensity (Filtrate)}}{\text{Fluorescence Intensity (Original)}} \ [\%] \quad (1)$$

ATR FT-IR

To determine secondary structure elements in peptide nanofibers ATR FT-IR was used. 50 µL of each peptide sample was lyophilized and spectra were recorded on a Bruker Tensor 27 spectrometer with a diamond crystal as ATR element (PIKE Miracle^{TM}, spectral resolution 4 cm^{-1}). Every sample was measured with 20 scans. Data were analyzed with OriginPro (OriginLab) software.

Primary neuronal cultures

Coatings

As positive control for neuronal and Schwann cell growth, a mixture of poly-L-lysine (PLL) and Cys-laminin (Cys-lam) was used. Cys-lam is part of the extracellular matrix protein laminin A chain (2091-2108) with an additional Cystein on its n-terminal end. For coating, the bottom of the wells were incubated with 100 µg/mL PLL in borate buffer for 1 h at 37° C. After incubation the PLL was removed and the well was washed 3 x with autoclaved ddH_2O. Following complete removal of ddH_2O, 20 µg/mL Cys-laminin in HBSS was coated on the glass bottom and incubated o/n at room temperature. SAP monomers were dissolved in DMSO (C = 10 mg/mL) to prevent fiber formation and stored at –20° C before usage. For fiber formation DMSO stocks were diluted in a polar solvent (1X PBS or ddH_2O for SAP^{1e}) to yield a final concentration of 1 mg/mL. After at least 18 h of incubation, the mature fiber solution was diluted in 10 mM Tris to get the desired concentrations ranging from 1 µg/ml to 50 µg/mL. 200 µL of SAP-solution were coated on the bottoms of the 24-well plates and dried o/n at RT. Directly before use, the wells were covered with 500 µL culture media.

Cell preparation

DRGs (dorsal root ganglia) of 7-9 weeks old C57BL/6 mice were isolated. As a first step, the spine with the rib cage of the mouse was removed and cleaned in ice cold PBS. Dissected DRGs were collected in Petri dishes with ice cold HBSS, dispensable tissue was removed and cleaned DRGs were stored on ice in 1 mL HBSS until further preparation. Following dissection, the DRGs were first centrifuged at 1000 rpm for 2 min at RT and the HBSS was replaced by 500 µL digestion solution (0.25% collagenase, 5% dispase dissolved in DMEM). For digestion, tubes containing DRGs and digest solution were incubated at 37° C for 1 h and flicked every 15 min. Afterwards the DRGs were spun down at 800 rpm for 2 min at RT and

then washed with 1 mL pre-warmed DRG media (DMEM/NBM ratio 1:1, supplemented with 10% FCS, 2% B27 supplement, 0.1% L-glutamine), following another centrifugation step at 800 rpm for 2 min at RT. Again, DRGs were washed with 1 ml DRG media and then transferred into falcon tubes. The solution was triturated 30 times with glass pipettes with whole diameter following 15 times triturating with glass pipettes with half the diameter. Afterwards, to get rid of tissue clumps, the solution settled for approximately 30 seconds and the supernatant was transferred to a new falcon tube. This was repeated once before the supernatant was centrifuged at 800 rpm for 5 min at RT. The resulting cell pellet was resuspended in 500 µL DRG culture media without NGF.

For CNS cultures, hippocampus of mice at post natal day 1-2 (P1-P2) and cerebellum of mice (P2-P4) were used. Mice were sacrificed by decapitation and their heads were immediately transferred into ice cold PBS. The head was then transferred into a Petri dish and the brain was dissected using microscissors. After dissection, the brain was put in another Petri dish containing cold HBSS and by the use of a stereomicroscope the cerebellum or both hippocampi were dissected. Subsequently, the tissue was digested with 2-3 mL trypsin per mouse for 10 min at 37°C. Digestion was stopped by replacing the trypsin with 1 mL pre-warmed HBSS. This was done two times and then the HBSS was completely removed following incubation with 1 mL pre-warmed DMEM supplemented with 10% horse serum (HS). Glass pipettes with whole diameter were first used for 1 min triturating followed by 1 min triturating with glass pipettes with half the diameter. After the solution was homogenized, the cells were centrifuged for 5 min with 600 rpm at RT. The supernatant was discarded and the cell pellet was resuspended in pre-warmed NMEM/B27 with Gentamycin (1:2000). The cell number was determined by counting with a Neubauer improved hemocytometer. For analysis of cell growth a total of 16 x

10^3 were platted on each well (⦸ 15 mm). The cells were cultured for 24 h in the Olympus microscope for time lapse recordings at 37°C and 5% CO_2.

Live cell imaging and analysis

To analyze cell attachment and growth, 5 x 10^3 DRG cells per well were seeded and incubated at 37°C and 5% CO_2. After 1.5 h incubation, the medium was replaced with fresh DRG culture medium (± NGF at 50 ng/mL). Afterwards, time-lapse recordings were performed by the Olympus microscope and the Olympus ScanR acquisition software. Cells were recorded for approximately 23 h, with pictures taken every 30 min at 37°C and 5% CO_2. Six positions per well were recorded with the UPLFLN-PH 10X objective. After cell staining, the plate was scanned by the microscope again. Using the ScanR acquisition software, 520 positions per well were recorded with the UPSALPO 10X objective. On each position the microscope performed the hardware autofocus (AF hardware) and fine autofocus (AF fine). After the recording, the cells could be analyzed via threshold detection using the corresponding ScanR analysis software. Different gates were defined to categorize the cells. First, a “Neuron” was defined by a co-localized DAPI and βIII tubulin signal. The detected DRG neurons were grouped in “round neurons” (208-908 μm^2), “small neurons” (908-1994 μm^2), “medium neurons” (1994-4161 μm^2) and “large neurons” (4161-18721 μm^2). A similar approach was used for CNS neurons and Schwann cells.

For measuring the neurite length of the cells, 20 cells per condition were chosen randomly. Images were taken with the Zeiss Axiovert 200 M microscope with a 10 X magnification. The neurite length was measured by using AxioVision software. For analysis, always the longest neurite of the neuron was chosen and measured from one tip of the neurite across the cell body to the other tip.

To determine neurite branching an automatic Sholl analysis using the Fiji plugin was used developed by Ferreira et al., 2014. The starting radius was set to 30 µm and the step size was determined to 20 µm. Ten cells per condition were analyzed. If possible, only cells with a neurite length ≥ 50 µm were chosen for analysis, otherwise the number of intersections was set to zero.

Stripe assay

Stripe assays were performed according to a published protocol (Knoll et al., 2007). Silicon matrices (provided by M. Bastmeyer, KIT, Karlsruhe, Germany) were washed in boiling autoclaved ddH_2O with 2 % SDS and afterwards in autoclaved ddH_2O only for 10 min each. After boiling, matrices were dried o/n at RT and subsequently positioned on glass coverslips (⦸ 15 mm). For the first stripes, 200 µg/mL SAP^{5c}-RITC were mixed with 10 µg/mL Alexa546 (goat) labeled antibodies (Invitrogen) to enhance fluorescence. 20 µL were injected with a Hamilton syringe per silicon matrix to create a pattern of alternating red-labeled stripes. Without removing the matrices, the SAP stripes dried o/n at RT in the dark. On the following day, the matrices were gently removed and the coverslips were either directly transferred into Nunc® 4 well plates and covered with 500 µL DRG culture medium with NGF, or stripes were covered with 50 µL unlabeled SAP^{5c} (final conc. 25 µg/mL), which dried o/n at RT in the dark. 20 x 10^4 DRG cells per coverslip were seeded and incubated at 37°C and 5% CO_2. Stripe assays were analyzed automatically by using an ImageJ plugin (Yamagishi et al., 2011).

Immunocytochemistry

After washing with PBS, cells were fixed with 4 % PFA in PBS for 15 min. Following fixation, the cells were washed three times with PBS and permeabilized with 0.1 %

Triton-X-100/PBS for 5 min. Then, the cells were washed again with PBS two times and subsequently incubated in blocking solution (2 % BSA in PBS) for 30 min at RT. Primary antibodies were diluted as described below in blocking solution and applied to the cells o/n at 4°C. The next day, the primary antibody solution was removed and the cells were washed three times with PBS. Secondary antibodies were also diluted in blocking solution 1:1500 and applied for 1 h at RT (anti-βIII tubulin, 1:2000, Covance; anti-S100b, 1:250, Abcam; Texas Red conjugated Phalloidin; 1:100, Molecular Probes; DAPI, 1:5000, AppliChem). Following two times of washing with PBS, the cell nuclei were stained with DAPI. After 5 min incubation with DAPI, the cells were washed with PBS again and mounted with pre-warmed Mowiol on microscope slides. The slides were dried o/n at RT and stored at 4°C.

Facial nerve axotomy

Adult C57BL/6 mice (10-12 weeks old) were anesthetized with isoflurane and subcutaneously injected with 5 mg/kg of the analgesic carprofen (Rimadyl 50 mg/mL). After shaving the right side of the mouse face, the skin on the right masseter muscle was cut with scissors. Subsequently, the buccal and marginal branch was cut with scissors. Directly after cutting, 1 µL per branch of RITC-labeled SAP-solution (1 mg/mL) or PBS for the control group was applied with a Hamilton syringe (26g) into the lesion site. To make sure that the SAPs will stay in the lesion site, the skin was not directly sutured, but the injury was protected from light for approximately 1 min so the labeled SAPs could stick to the tissue. For quantification of RITC signals in the lesion site, we used Axiovision software. Subsequently, the skin was closed with an Ethicon K871H suture and successfully performed surgery was controlled by impaired whisker movement. The surgery was performed unilaterally, so that the uninjured contralateral side of the mouse could serve as internal control.

To asses axonal regeneration of the injured facial nerve the retrograde axonal tracer Fluoro-Gold (FG; Milipore) was used. A 4 % solution of FG in ddH_2O was injected in both whisker pads by using a Hamilton syringe. For each side, a total of 4 µL FG solution was used and injected at two positions in the upper part of the whisker pad and at two positions in the lower part. FG injection was performed one day prior to sacrificing the mice. All experiments in this study were reviewed and approved and were in accordance with regulations by the local veterinary authorities (Regierungspräsidium Tübingen, Germany).

Whisker movement

The whisking was recorded one day before facial nerve transection and on different time points during regeneration. Cohorts with a regeneration period of 21 days were recorded at 1, 4, 9, 11, 14, 16 and 18 days post injury (dpi). For recordings the mice were placed under a high-speed camera (Basler acA1300-60gc) on an illuminated plate. Video recordings lasted for 60 s with a frame rate of 100 Hz. For analyzing the recorded whisking of the mice, the videos were reviewed and a sequence of 1s duration was further processed with Templo Software (CONTEMPLAS GmbH, Germany). The selected video sequences were analyzed by Vicon Motus 2D software (CONTEMPLAS GmbH, Germany). Different parameters of whisker movement were measured by the Vicon Motus 2D software, including angular range, velocity and acceleration. The angular range was defined as the difference between minimum and maximum deflection of the vibrissae. The overall angular sum of whisker movement during 1 s was calculated with a custom MATLAB program, where all deflections above a threshold of 10° were summed up for lesion and control side.

Immunohistochemistry

Tissue was fixed in 4% formaldehyde (FA) for three days, followed by preparation of 5µm paraffin microtome slices. Immunohistochemistry was performed using Biotin (1:500; Vector Laboratories) or Alexa Fluor (1:500; Invitrogen) conjugated secondary antibodies and peroxidase-based detection systems using the ABC complex (Vector Laboratories) and DAB as substrate. Primary antibodies included anti-FG (rabbit, 1:5000, AB153; Millipore), anti-S100b (rabbit, 1:1000; Abcam), anti-VAChT (goat, 1:1000, Merck), anti-MBP (mouse, 1:1500, Covance), anti-βIII tubulin (rabbit, 1:1000, Covance), DAPI (1:5000, AppliChem)

Scanning Electron Microscopy

The SAPs were coated on glass slips as described above and dried overnight. Primary neuronal cells from adult mouse DRGs were dissected as described before. Neurons were cultivated for 3 DIV without additional NGF in the growth medium. The next steps were performed by the electron microscopy core facility at Ulm University and will only be described briefly. For a more detailed protocol see (Walther et al., 2010). First, the peptides were fixed for 1 h with a fixation solution containing glutaraldehyde. Then they were washed three times and fixed additionally with 4% osmiumtetroxyd. Any remaining water was removed by an increasing alcohol series. Afterwards, the alcohol was replaced by CO_2. The probes were dried by critical point drying. There, the probes were dried above the critical point of CO_2, where liquid and gas phase cannot be separated. By slowly decreasing the pressure while keeping the temperature constantly supercritical, the probes were dried without destroying the natural structure. To increase the electrical conductivity, the probes were vaporized with a platinum layer. Probes were analyzed with the Hitachi S-5200 Scanning Electron Microscope (Hitachi High Technologies Corporation).

Data Mining of Peptides

We modeled amino acids as building blocks with two important physical properties relevant for this problem: hydrophobicity and charge. An amino acid can be hydrophobic (H^0) or hydrophilic. The hydrophilic amino acids can be uncharged (P^0), positively charged (P^+) or negatively charged (P^-). This coarse-graining of amino acids provided us with four types of amino acids (see Table S2 for classification of amino acids into these categories).

To make the library of amino acid sequences, we noted that each position in a sequence of amino acids can be occupied by one of the four types of amino acids. Consequently, a 3-length sequence can be one of the 4x4x4=64 types. We made a library of all 3, 4, and 5 amino acid long sequence units to proceed systematically. Combinatorially, there are 1344 such sequence units. Longer polypeptide sequences were constructed by repeating the same-length units. This procedure allowed us to make a large number of sequences with a fixed and reproducible protocol. As an example, $H^0H^0P^+$ and $P^+P^+P^-P^+$ are one trimeric and one tetrameric unit, respectively, in our representation. The longer sequences they make are $H^0H^0P^+H^0H^0P^+$… and $P^+P^+P^-P^+P^+P^+P^-P^+$ … Note that each sequence unit can represent multiple amino acid sequences. We also used the fact that the cell membranes are negatively charged in the experiments and the overall positively charged SAPs have higher activity. In our library, the overall net charge of a constructed sequence was constrained to be positive to make accurate predictions. This reduced the number of considered sequences from 1344 to 501.

We then compared how similar each of these sequences are to SAPs. The similarity between an experimental SAP, denoted X, and a constructed sequence, denoted Y, was quantified by the overlap index(I) defined as

$$I(X,Y) = \frac{|X \cap Y|}{\min(|X|,\ |Y|)}. \quad (2)$$

The numerator in Eq. (2) is the number of position-matched amino acids between sequences X and Y. For example, there are 2 matches between the sequences $P^+P^+P^-P^+$ and $P^+P^+H^0P^-$. The denominator is the minimum among the lengths of $P^+P^+P^-P^+$ and $P^+P^+H^0P^-$, which is 4 as they are of the same length. Thus, $I = \frac{2}{4} = 0.5$ for these two sequences.

As mentioned before, the sequences that have high overlap index with SAPs with high activity and low overlap index with sequences with low or medium activity are the most promising sequences to show high activity in experiments. In Figure S6, these most promising sequences are represented by the points on the lower-right corner.

To rank the sequences, we formulated the index:

$$Q = I(X, Y_h)_{Av} - I(X, Y_l)_{Av} - I(X, Y_m)_{Av}. \quad (3)$$

In the above equation X represents a sequence from the library, Y_h is a high-activity sequence, Y_l is a low activity sequence and Y_m is a medium activity sequence. The averaging was done over the respective activity types. We conjecture that sequences with high values of Q has the potential to show higher activity in the experiments.

Once we ranked the constructed sequences, we found out relative occurrences of amino acid types present in each position of the sequences with high values of the index Q. The resulting histograms, drawn for sequences having the highest 5, 10, and 15 Q values, are shown in Figure S7. Based on this analysis, we found that in the top-ranking sequences the recurring pattern is $H^0P^+H^0P^+H^0$. The third position is a bit ambiguous as it varies when we consider the best 15 sequences. The observed variability stems from the limited dataset of SAP sequences. To get longer

polypeptide sequences one needs to repeat the predicted unit like $H^0P^+H^0P^+H^0H^0P^+H^0P^+H^0$.

Next, we compared the predicted pattern, namely $H^0P^+H^0P^+H^0$, that we obtained from our own dataset with peptide sequences reported in the literature that were shown to support neuronal growth and determined how well the identified pattern matches with these sequences. We selected a total of 18 peptide-containing molecules from the literature that were used as coatings in neuronal cultures. We found that two classes of molecules, peptides belonging to the RADA family and peptide amphiphiles (PAs), were used most frequently in relevant literature studies. In order to be accessible to our data mining approach, molecules need to be represented as pure amino acid sequences. However, PA molecules feature an alkyl tail coupled to a peptide sequence. We chose to represent the palmityl group of PAs as 4 leucine units in the simplified sequence used for comparing with our dataset. Likewise, small chemical modifications such as the amidated *C*-terminus of certain peptides are not represented in the translated sequence. The *in vitro* data provided in the literature uses different culturing conditions and even different cell types, which prevents a direct evaluation of “neuronal activity” as defined in our work and we assigned medium or high activity after considering the presented data. Nevertheless, we believe that a comparison with our dataset can give valuable insight.

For comparison with the literature sequences, we first performed an out-of-sample analysis. We randomly split our SAP dataset into one larger set (training set) containing 75% and one smaller set (test set) containing 25% of the whole dataset using the scikit-learn package (Pedregosa et al., 2011). We then identified the most-occurring pattern by applying our algorithm only on the training set and measured its overlap with SAPs only from the test set. Repetition of this analysis allows us to: a) verify that, on average, $H^0P^+H^0P^+H^0$ is the most-occurring pattern - indicating the

robustness of our predicted pattern - and b) find the average overlap of the predicted pattern with the experimental SAPs. After repeating the test-train splitting 2000 times and collecting the overlap data for each of them, we were able to obtain reliable statistics. Figure S8 shows that indeed, on average, $H^0P^+H^0P^+H^0$ is the most-occurring pattern in the high-activity SAPs and, thus, our prediction is robust. Figure S9 shows the overlap statistics. First, we note that $H^0P^+H^0P^+H^0$ has better overlap with high activity SAPs than low activity SAPs, which confirms that the predicted pattern works well when applied to a high-activity SAP from a randomly chosen test set from our data. However, when we compare the predicted pattern with the high-activity literature sequences, we obtain a broad range of overlap values. The best match is found for P7, reaching a value of 0.45, while some other sequences have a low overlap value of around 0.1. Interestingly, the PA molecules show moderate overlap with the predicted pattern (see P1, P6, P10, P14-P16 in Table S3), while peptides belonging to the RADA family generally show a low overlap (see P3, P4, P17, P18 in Table S3).

The observed moderate to low overlap of the predicted pattern with the peptides from PA family or RADA family is not unexpected since all of the SAPs that we used to train our data-mining model have a net positive charge and repeating coarse-grained amino acid units, while many of the peptides from these families are negative or neutral and have quite different structure and thus belong to very different regions of the sequence space than that we considered. For peptide P7, which falls in the broad structural class of the SAPs, the match is reasonable. We expect that augmenting the training of our proposed algorithm with a list of peptides having different structures but one unifying feature, namely high neuronal regeneration activity, will considerably enhance the predictive power of this data-mining approach for the

current problem. This study thus motivates larger data-mining studies across peptide sequences.

Supplementary Tables

Table S1

Collected fractions of all peptides after purification with HPLC. Calculated mass and found m/z of all peaks with an intensity of at least 10 % in relation to the main peak.

#	SAP name	fraction collected [min]	calc. exact mass [g/mol]	*m/z* found
1	SAP^{1a}	10.17 to 10.72	982.69	983.70 $[M+H]^+$, 1005.68 $[M+Na]^+$
2	SAP^{1b}	10.40 to 10.93	982.69	983.70 $[M+H]^+$, 1005.68 $[M+Na]^+$
3	SAP^{1c}	11.06 to 11.30	967.68	968.69 $[M+H]^+$, 990.67 $[M+Na]^+$
4	SAP^{1d}	9.82 to 10.29	741.51	742.52 $[M+H]^+$, 764.50 $[M+Na]^+$
5	SAP^{1e}	12.81 to 13.66	963.58	964.59 $[M+H]^+$, 986.57 $[M+Na]^+$, 1002.54 $[M+Ka]^+$, 1008.55 [unknown]
6	SAP^{2a}	12.04 to 13.02	1137.60	1138.61 $[M+H]^+$, 1160.59 $[M+Na]^+$, 1176.56 $[M+K]^+$
7	SAP^{2b}	10.64 to 11.41	843.46	844.47 $[M+H]^+$, 866.45 $[M+Na]^+$
8	SAP^{2c}	10.95 to 11.90	1118.63	1119.63 $[M+H]^+$, 1141.62 $[M+Na]^+$
9	SAP^{2d}	10.09 to 11.08	1088.55	1089.55 $[M+H]^+$, 1105.55 $[M+O+H]^+$, 1111.54 $[M+Na]^+$
10	SAP^{2e}	10.78 to 11.38	946.47	947.48 $[M+H]^+$, 1136.52 $[M+O+H]^+$, 1892.94 $[2M-2H+H]^+$
11	SAP^{3a}	10.65 to 11.29	1300.73	1301.74 $[M+H]^+$, 1317.74 $[M+O+H]^+$, 1323.55 $[M+Na]^+$, 1349.73 [unknown]
12	SAP^{3b}	10.29 to 11.28	1403.74	1404.75 $[M+H]^+$, 1420.74 $[M+O+H]^+$, 1426.73 $[M+Na]^+$, 1436.74 [unknown], 1452.73 [unknown], 2807.47 $[2M-2H+H]^+$
13	SAP^{3c}	9.96 to 10.49	986.59	987.60 $[M+H]^+$, 1003.60 $[M+O+H]^+$
14	SAP^{4a}	9.81 to 10.79	1089.60	976.57 $[M-ASN+H]^+$, 1090.61 $[M+H]^+$, 1112.59 $[M+Na]^+$, 1196.65 $[M+Anisyl+H]^+$, 2065.15 [unknown], 2179.20 $[2M-2H+H]^+$ 2201.18 $[2M-2H+Na]^+$
15	SAP^{4b}	n.d.		n.d.
16	SAP^{4c}	10.25 to 10.67	1089.60	976.57 $[M-ASN+H]^+$, 1090.61 $[M+H]^+$, 1003.60 $[M+O+H]^+$, 2065.16 [unknown], 2179.20 $[2M-2H+H]^+$.
17	SAP^{4d}	9.63 to 10.05	844.52	845.53 $[M+H]^+$, 867.51 $[M+Na]^+$, 1034.57 [unknown], 1688.03 $[2M+H]^+$, 1710.01 $[2M+Na]^+$
18	SAP^{4e}	n.d.	844.52	845.53 $[M+H]^+$, 1688.03 $[2M+H]^+$
19	SAP^{4f}	n.d.	1403.74	n.d.
20	SAP^{5a}	10.00 to 10.59	1417.75	1418.76 $[M+H]^+$, 1451.85 [unknown], 1469.86 [unknown], 1485.85 [unknown]
21	SAP^{5b}	9.98 to 10.53	1314.74	1201.71 $[M-ASN+H]^+$, 1315.75 $[M+H]^+$, 1337.73 $[M+Na]^+$
22	SAP^{5c}	9.54 to 10.52	1172.67	1173.68 $[M+H]^+$, 1224.78 $[unknown]^+$, 1279.72 $[M+Anisyl+H]^+$, 2345.34 $[2M-2H+H]^+$
23	SAP^{5d}	10.14 to 11.12	1628.88	1515.85 [M-ASN+H], 1629.89 $[M+H]^+$, 1677.88 [unknown]
24	SAP^{6a}	9.07 to 9.57	1069.66	1070.67 $[M+H]^+$, 1092.65 $[M+Na]^+$
25	SAP^{6b}	10.06 to 10.42	1172.67	1173.68 $[M+H]^+$, 1279.72 $[M+Anisyl+H]^+$, 2345.33 $[2M-2H+H]^+$
26	SAP^{7a}	12.19 to 13.17	2275.28	2140.23 [unknown], 2277.29 $[M+H]^+$, 2299.27

				$[M+Na]^+$
27	SAP[7b]	11.36 to 12.35	1354.88	922.54 [unknown], 1227.80 $[M-Lys+H]^+$, 1355.89 $[M+H]^+$, 1387.88 [unknown]
28	SAP8[a]	n.d.	988.49	989.50 $[M+H]^+$, 1005.49 $[M+O+H]^+$, 1011.48 $[M+Na]^+$, 1027.48 $[M+K]^+$

Table S2

Classification of amino acids based on their hydrophobicity and side-chain charge (at pH 7.4)

Name	**Type**	**Kyte-Doolittle hydropathy index** (Kyte and Doolittle, 1982)	**Charge**	**Example**
H^0	Hydrophobic	Positive	0	Alanine, Cysteine, Phenylalanine, Isoleucine, Leucine, Methionine, Valine
P^+	Positively charged	Negative	+1	Histidine, Lysine, Arginine
P^-	Negatively charged	Negative	-1	Aspartic acid, Glutamic acid
P^0	Hydrophilic	Negative	0	Glycine, Asparagine, Proline, Glutamine, Serine, Threonine, Tryptophan, Tyrosine

Table S3

List of peptide sequences found in the literature with high or moderate neuronal activity for comparison with SAP dataset.

Name	Original Sequence	Simplified Sequence	Neuro Activity	Reference
P1	Palmitoyl-VVAAEE-NH2	LLLLVVAAEE	high	Angeloni et al., 2011; Berns et al., 2016; Choe et al., 2017; Berns et al., 2014
P2	RADARADARADARADA	RADARADARADARADA	high	Ellis-Behnke et al., 2006; Francis et al., 2016
P3	AcN-RARADADARARADADA-GG-RPKPQQFFGLM	RARADADARARADADA-GGRPKPQQFFGLM	high	Kim et al., 2013
P4	RARADADARARADADA	RARADADARARADADA	high	Kim et al., 2013
P5	RAEARAEARAEARAE	RAEARAEARAEARAE	medium	Liang et al., 2015
P6	Palmitoyl-VVVAAAEEE-NH2	LLLLVVVAAAEEE	high	Greene et al., 2018
P7	CCRRIKVAVWLC	CCRRIKVAVWLC	high	Li et al., 2014
P8	Palmitoyl-AAAGGGEIKVAV	LLLLAAAGGGEIKVAV	high	Zou et al., 2009
P9	KKQLQLQLQLQLQLKK	KKQLQLQLQLQLQLKK	high	Liu et al., 2013
P10	Palmitoyl-VVAAEE-ADEGVFDNFVLK	LLLLVVAAEEADEGVFDNFVLK	high	Berns et al., 2016
P11	RADARADARADARADA-GG-CQAASIKVAV	RADARADARADARADA-GGCQAASIKVAV	high	Tavakol et al., 2016, Tavakol et al., 2017
P12	RADARADARADARADA-RGIDKRHWNSQ	RADARADARADARADA-RGIDKRHWNSQ	high	Shi et al., 2016
P13	Palmitoyl-VVAAEEEEGIKVAV-COOH	LLLLVVAAEEEEGIKVAV	high	Berns et al., 2014
P14	Palmitoyl-VVAAEEEEGVVIAK-COOH	LLLLVVAAEEEEGVVIAK	medium	Berns et al., 2014
P15	Palmitoyl-VVAAEERGDS-NH2	LLLLVVAAEERGDS	medium	Berns et al., 2014
P16	Palmitoyl-VVAAEERSDG-NH2	LLLLVVAAEERSDG	medium	Berns et al., 2014
P17	RADARADARADARADA-GG-CTDIKGKCTGACDGKQC	RADARADARADARADA-GGCTDIKGKCTGACDGKQC	high	Lu et al., 2018
P18	RADARADARADARADA-GG-RGIDKPHWNSQ	RADARADARADARADA-GGRGIDKPHWNSQ	high	Lu et al., 2018

Table S4

Summary of several biophysical parameters along with SAP's potential to stimulate neuronal growth

SAP	Neuronal Activity	intermolecular b-content	Conversion Rate [%]	Diameter
SAP^{1d}	low	++	5	n/a
SAP^{1e} (PBS)	medium	++	30	n/a
SAP^{2b}	medium	--	83	-
SAP^{2e}	high	++	95	++
SAP^{5c}	high	++	80	++
SAP^{6a}	low	-	n/a	+
SAP^{7a}	medium	--	96	n/a
SAP^{7b}	low	---	92	n/a

Supplementary Figures

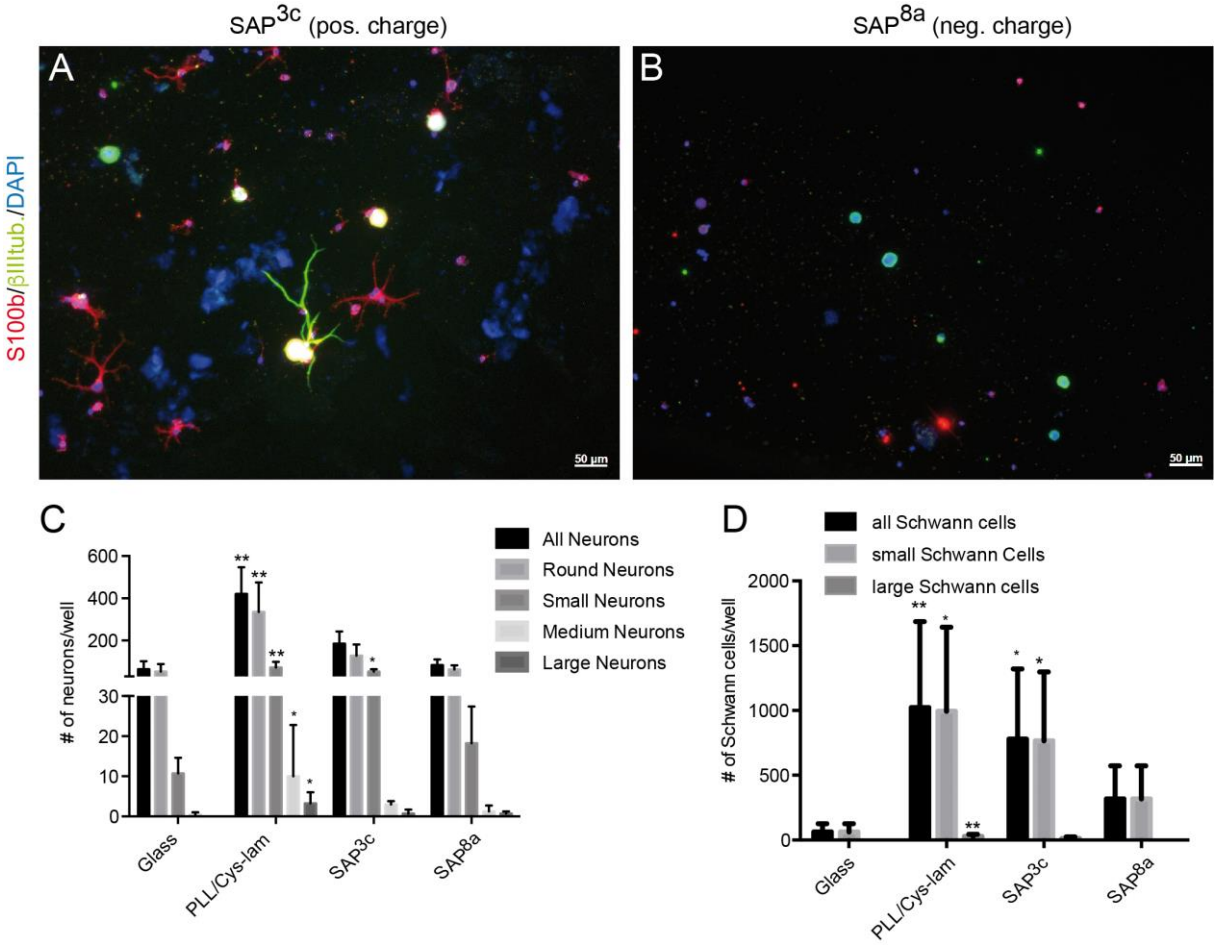

Figure S1

Negatively charged SAPs do not mediate cell adhesion or growth

(A, B) DRG neurons were cultivated on coverslips coated with SAP^{3c} (positively charged) or SAP^{8a} (negatively charged). Cells were stained with S100b and βIII tubulin to label Schwann cells and neurons, respectively. In contrast to SAP^{8a} (B), neurons adhered to and grew on SAP^{3c} (A).

(C, D) Quantification neuronal (C) or Schwann cell (D) growth on glass, PLL/Cys-lam, SAP^{3c} and SAP^{8a}. Data show mean ± SD of four independent cultures.

Scale-bar (A, B) = 50 µm

SAP^{1a}

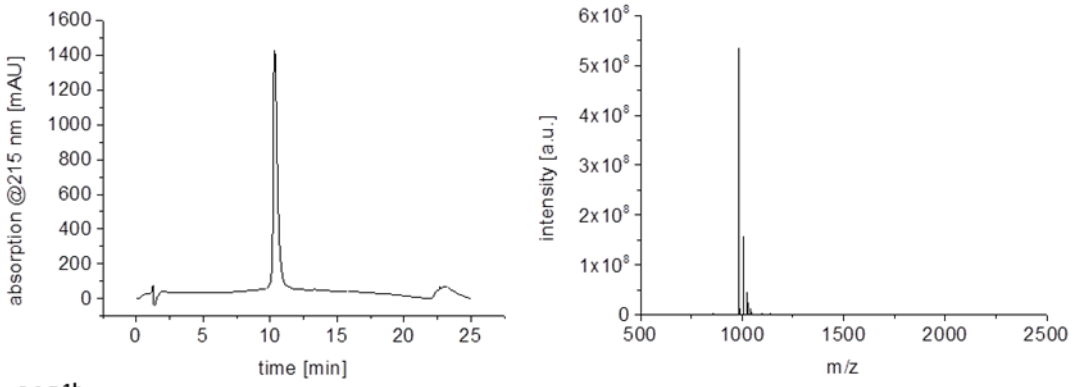

SAP^{1b}

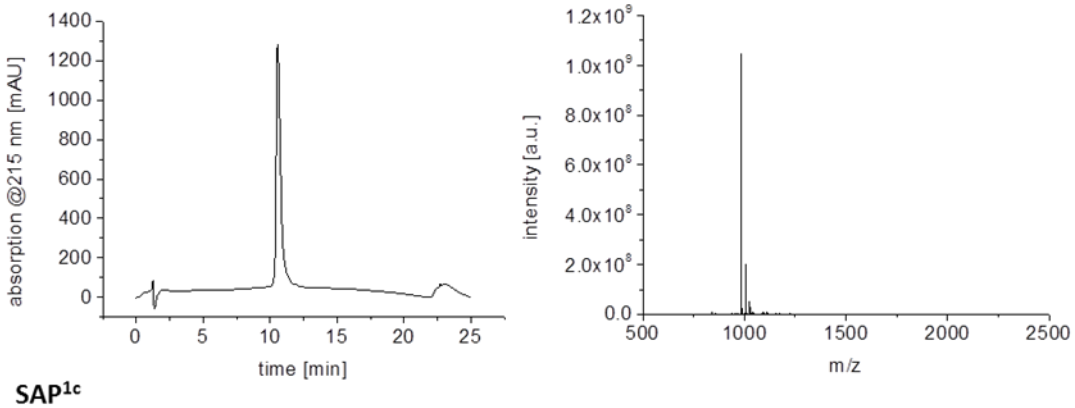

SAP^{1c}

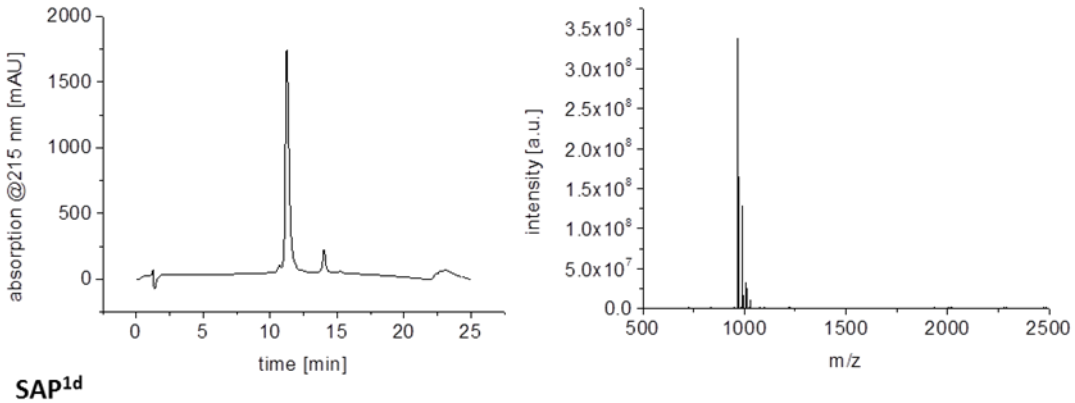

SAP^{1d}

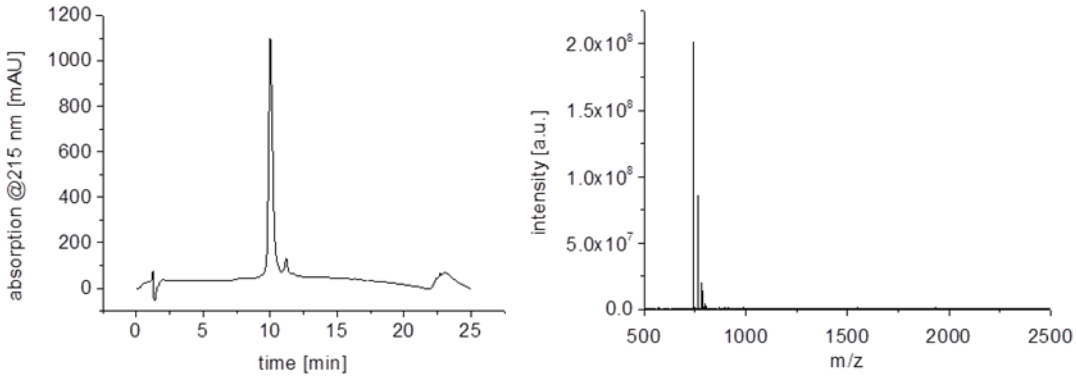

SAP^{1e}

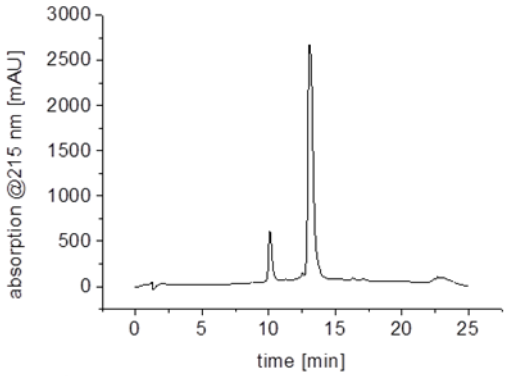

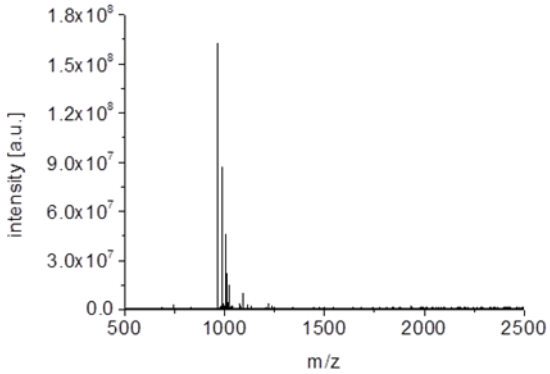

SAP^{2a}

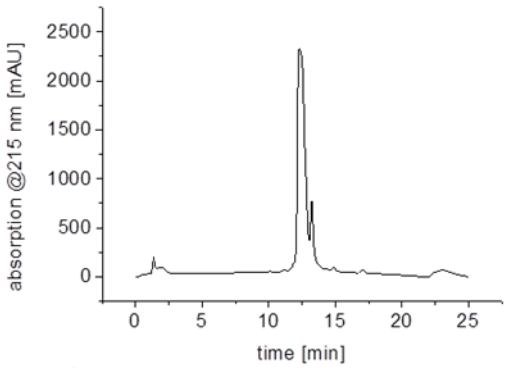

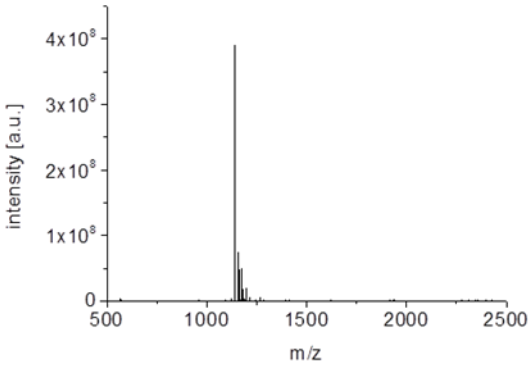

SAP^{2b}

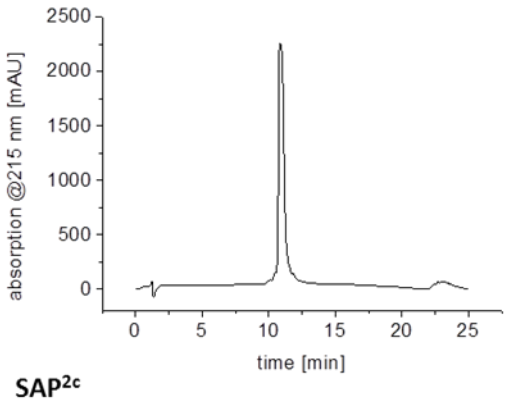

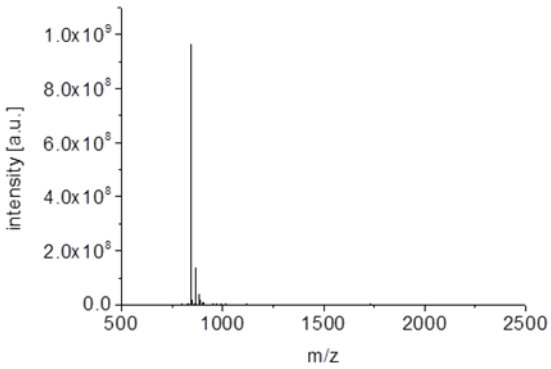

SAP^{2c}

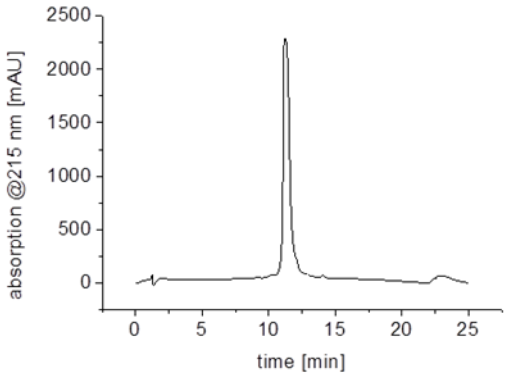

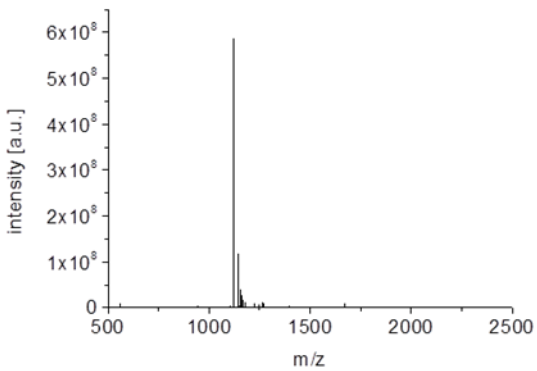

SAP^{2d}

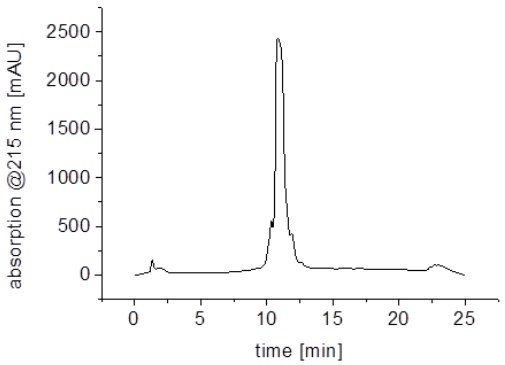

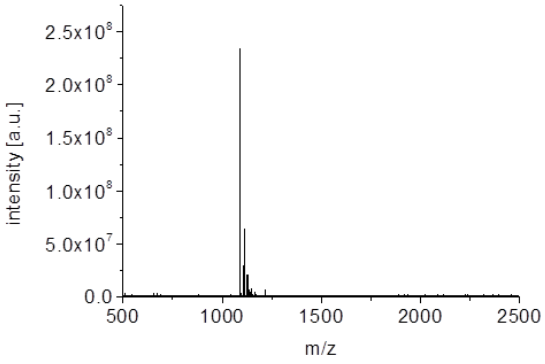

SAP^{2e}

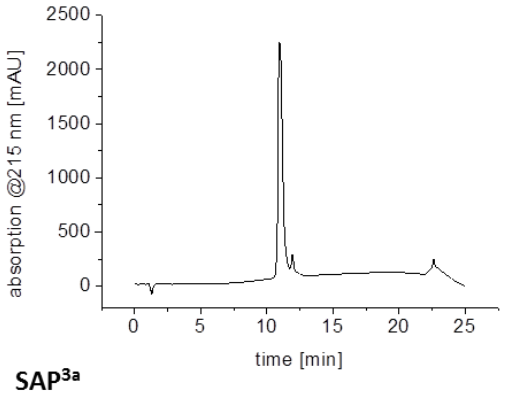

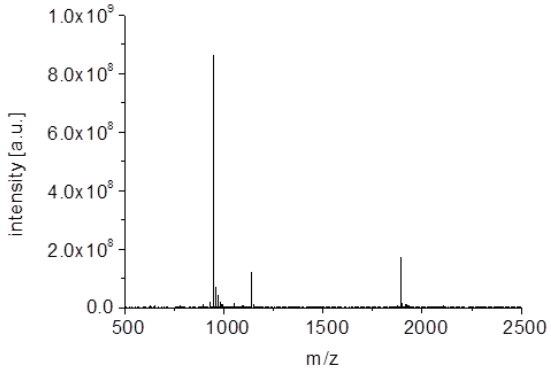

SAP^{3a}

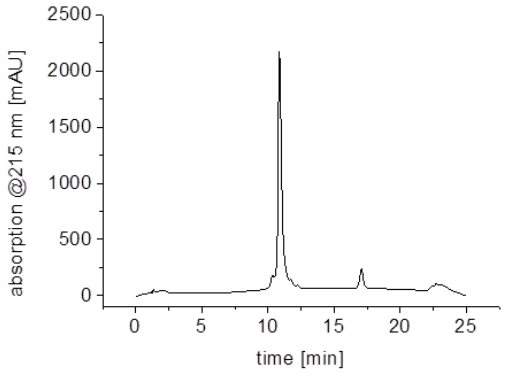

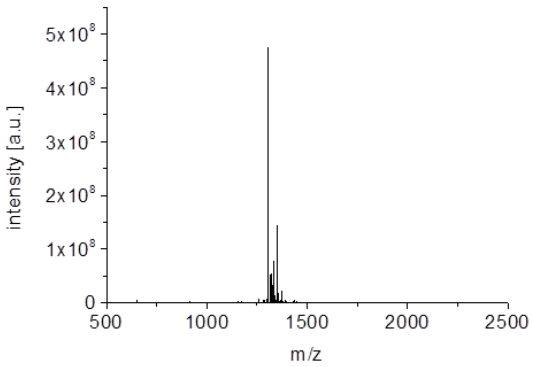

SAP^{3b}

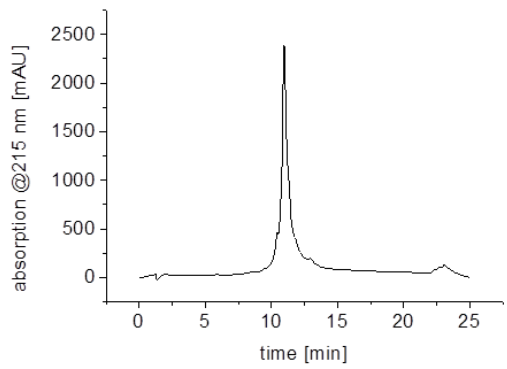

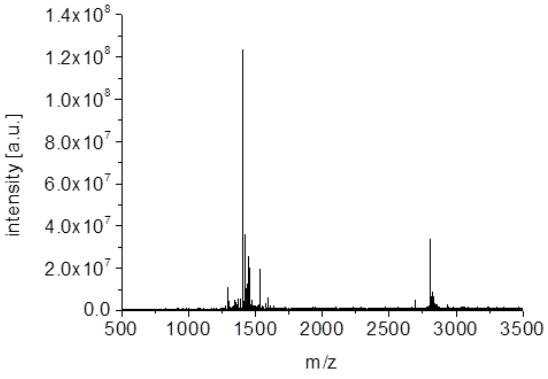

SAP^{3c}

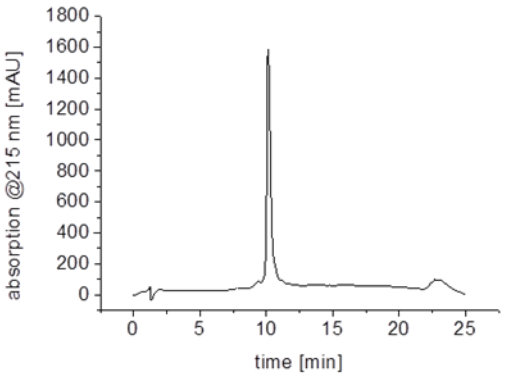

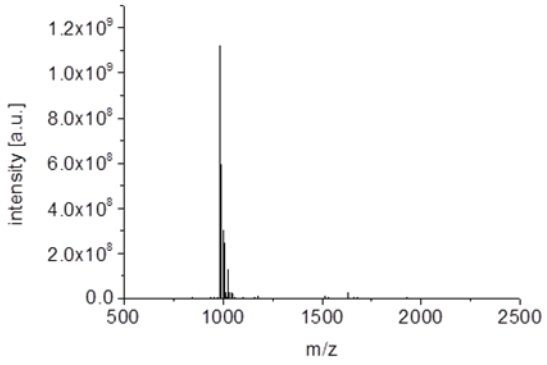

SAP^{4a}

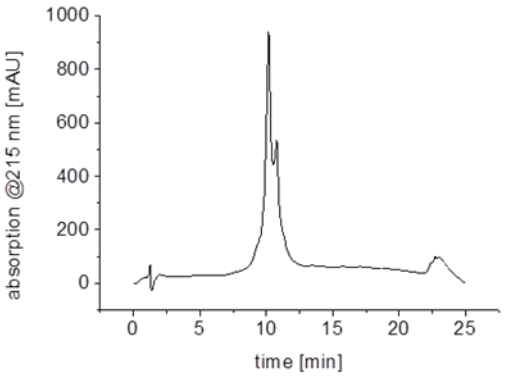

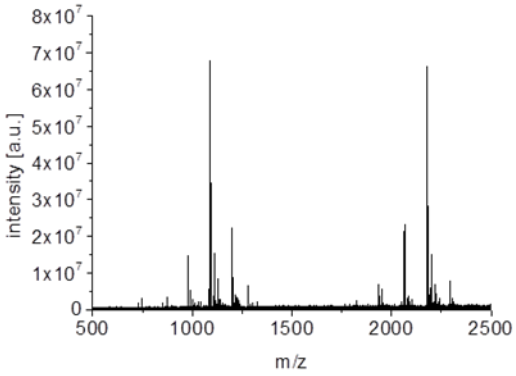

SAP^{4c}

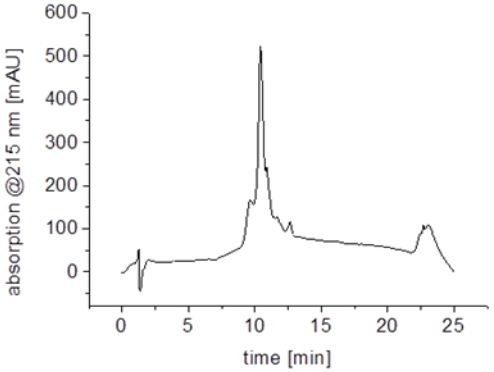

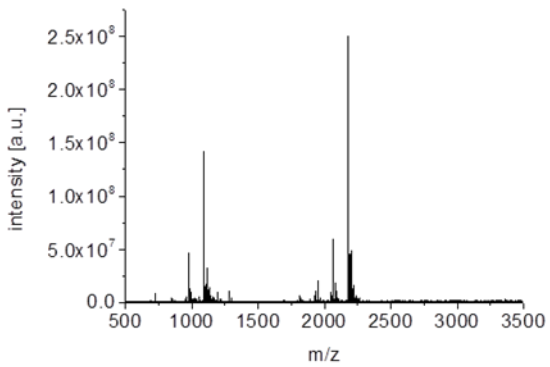

SAP^{4d}

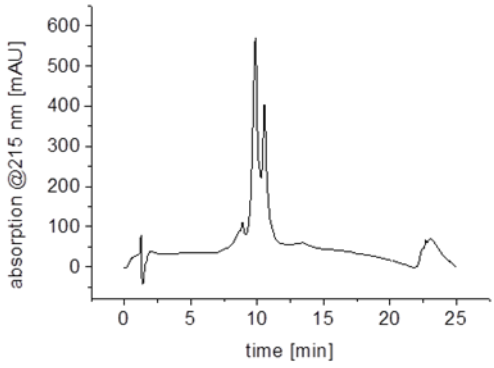

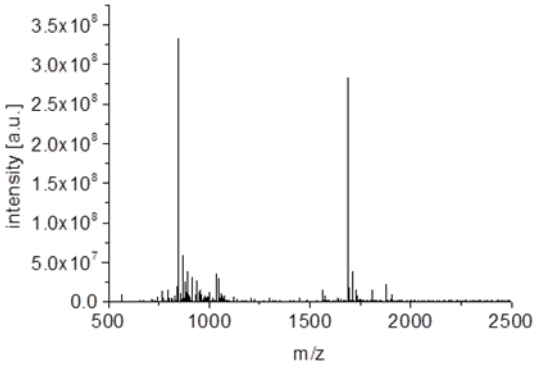

SAP^{4e}

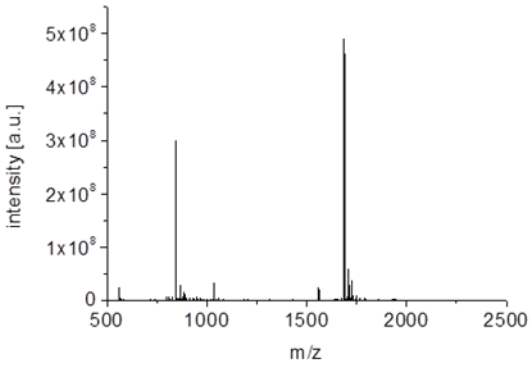

SAP^{5a}

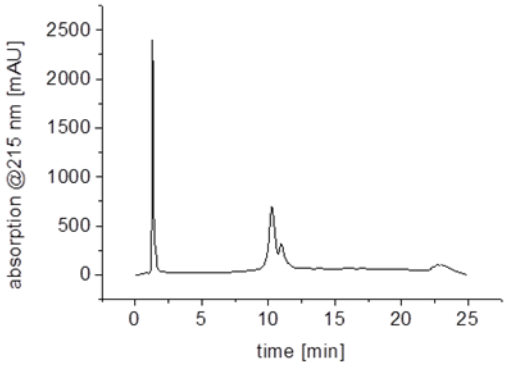

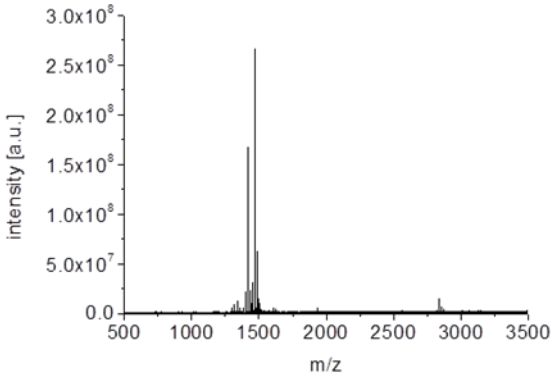

SAP^{5b}

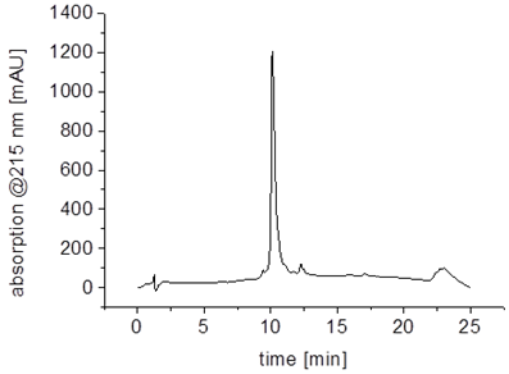

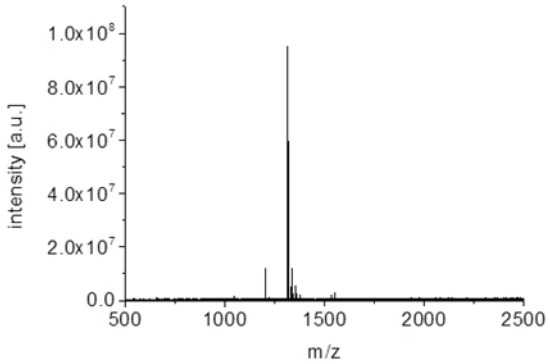

SAP^{5c}

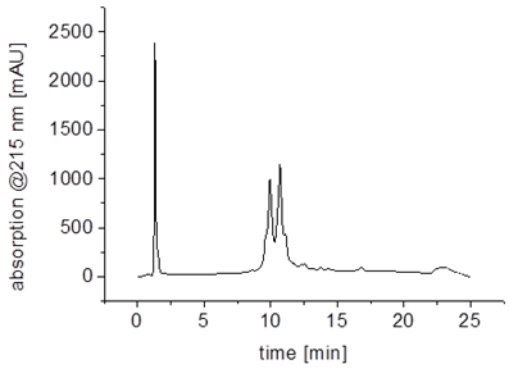

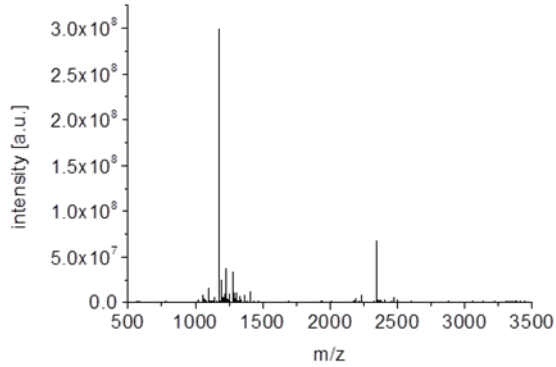

SAP^{5d}

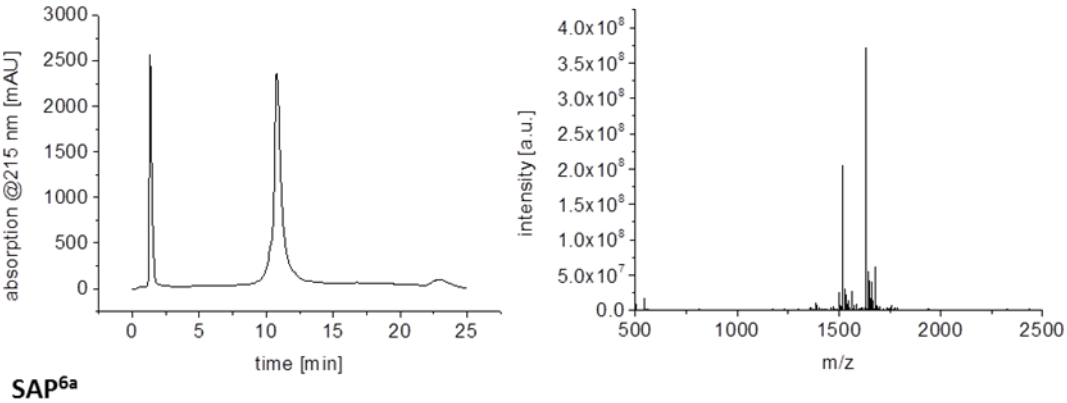

SAP^{6a}

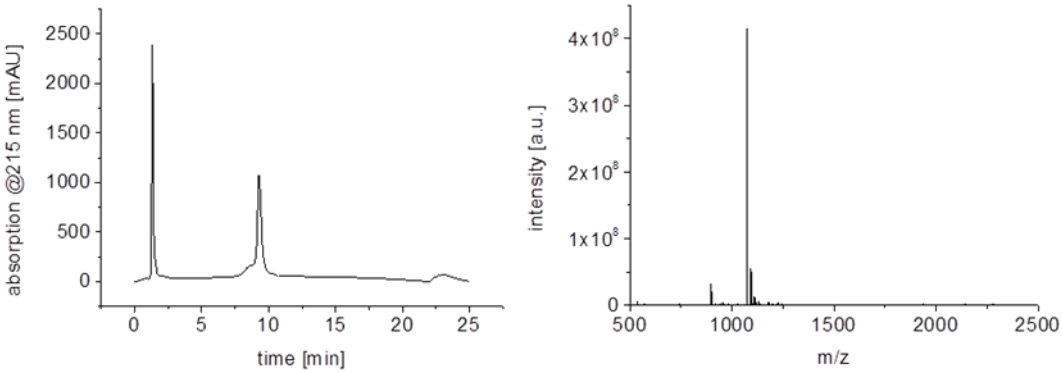

SAP^{6b}

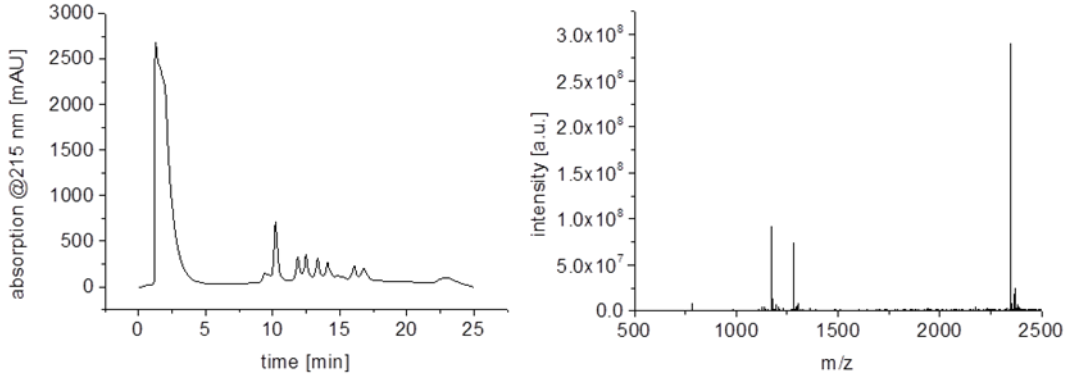

SAP^{7a}

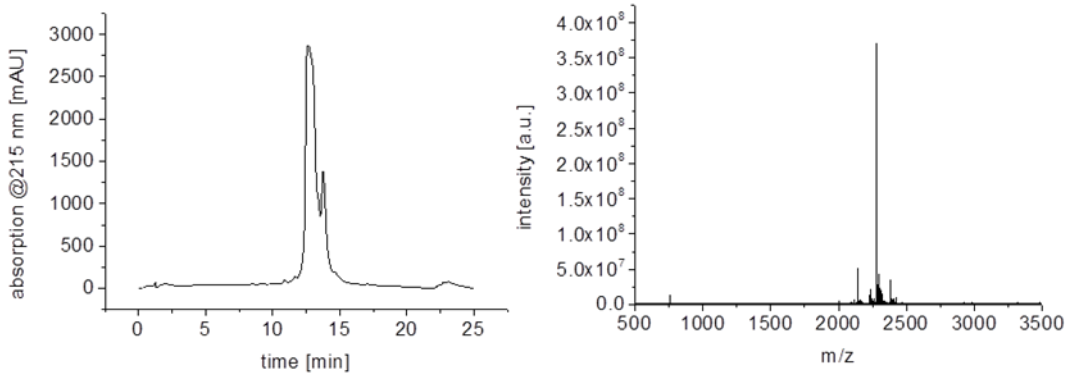

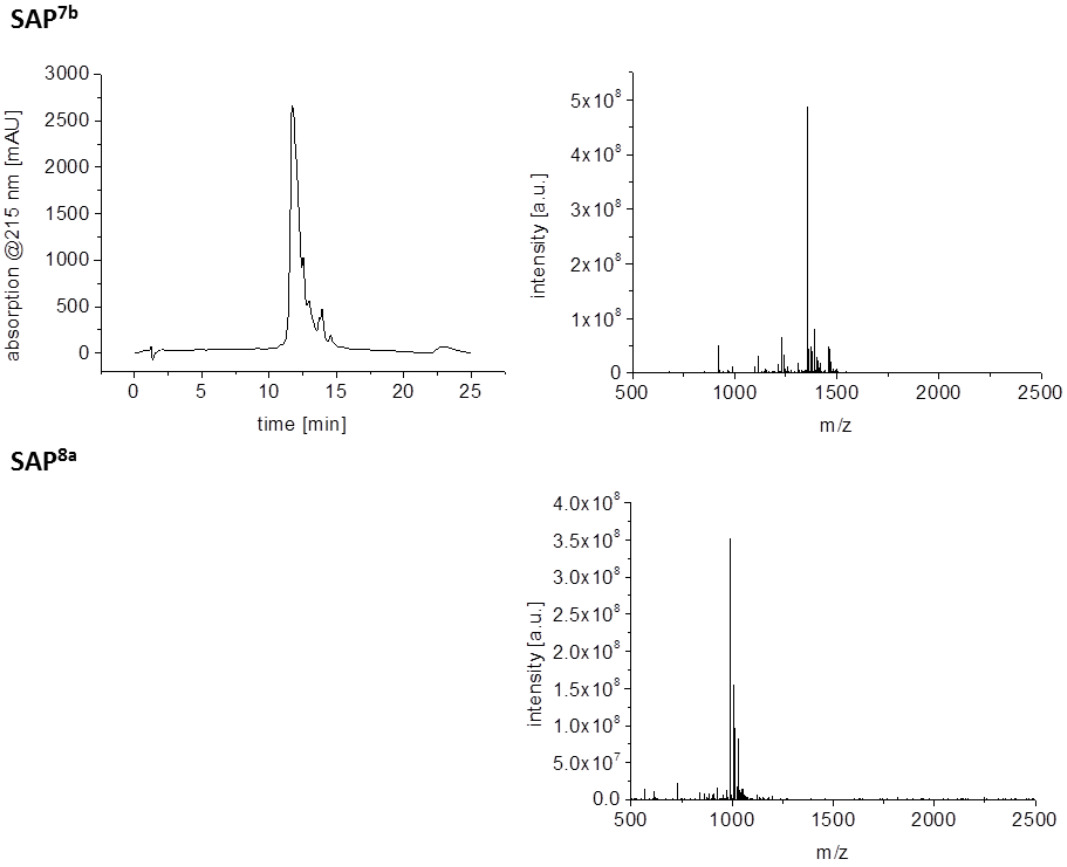

Figure S2

HPLC chromatograms of peptides (left side). MALDI-TOF mass spectra of peptides (right side). All data are summarized in Table S1.

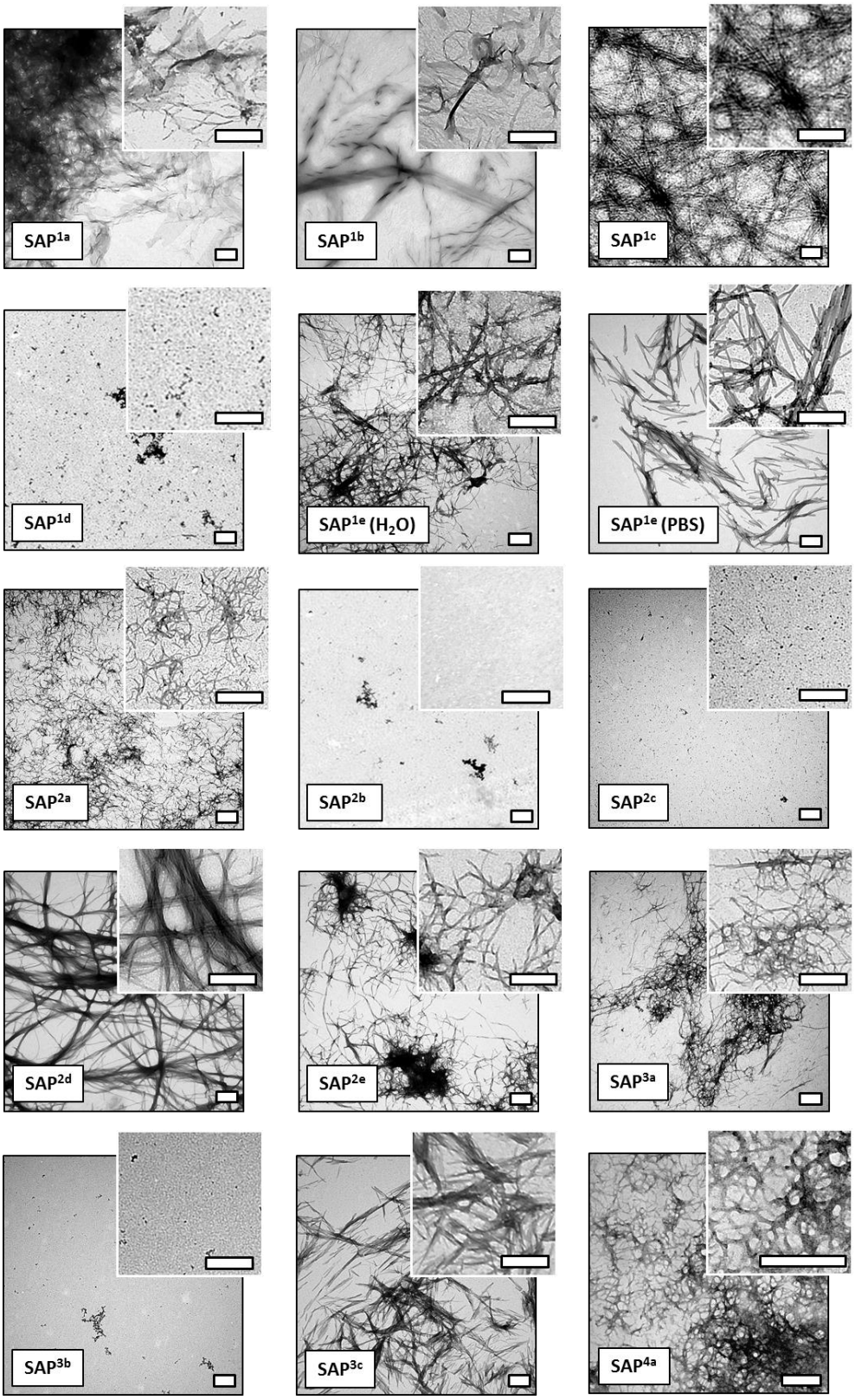
SAP1a
SAP1b
SAP1c
SAP1d
SAP1e (H2O)
SAP1e (PBS)
SAP2a
SAP2b
SAP2c
SAP2d
SAP2e
SAP3a
SAP3b
SAP3c
SAP4a

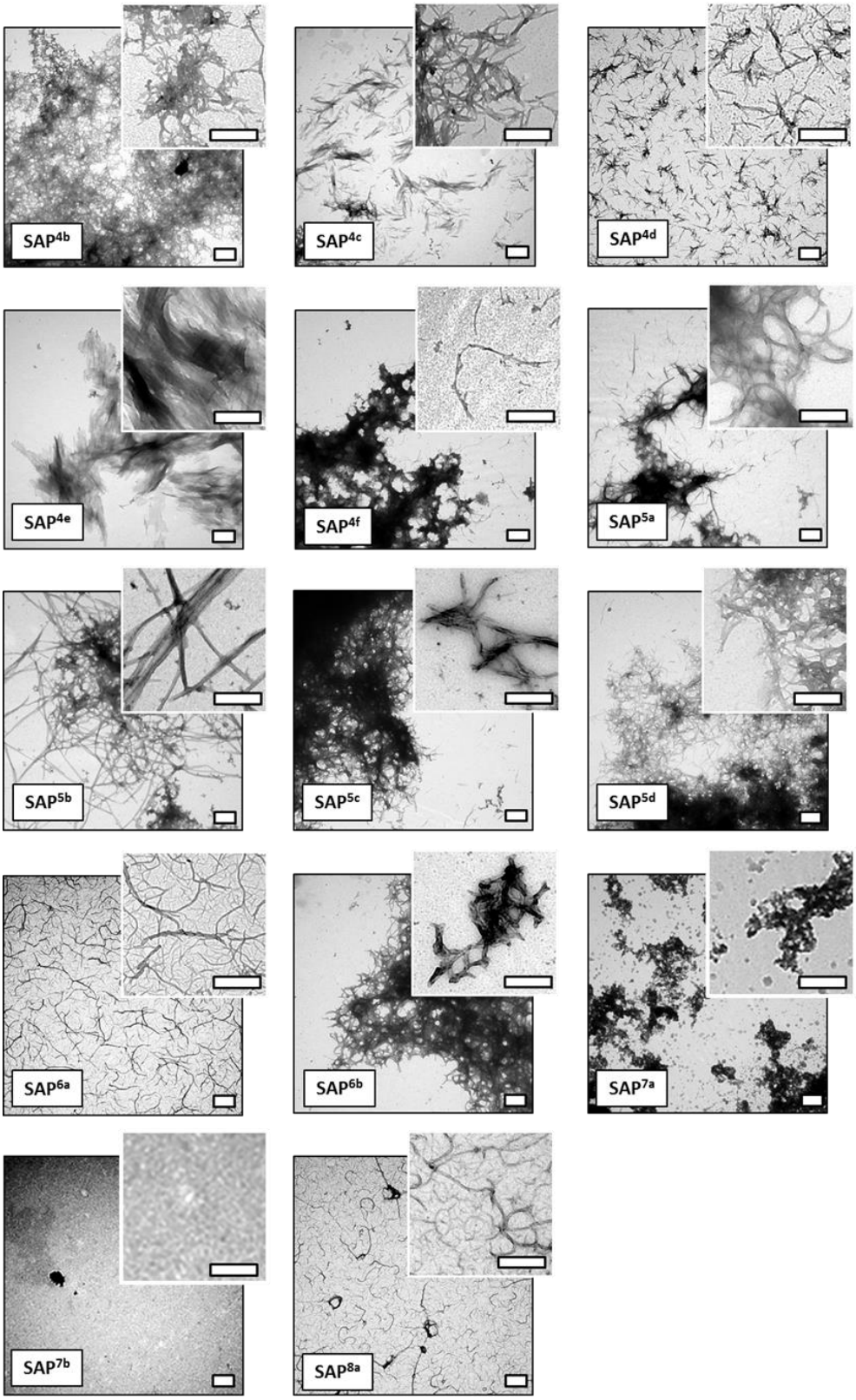

Figure S3

Transmission electron microscopy images of all peptides after 1 day of incubation in PBS (ddH_2O) with a final concentration of 1 mg/mL. Scale-bars = 250 nm.

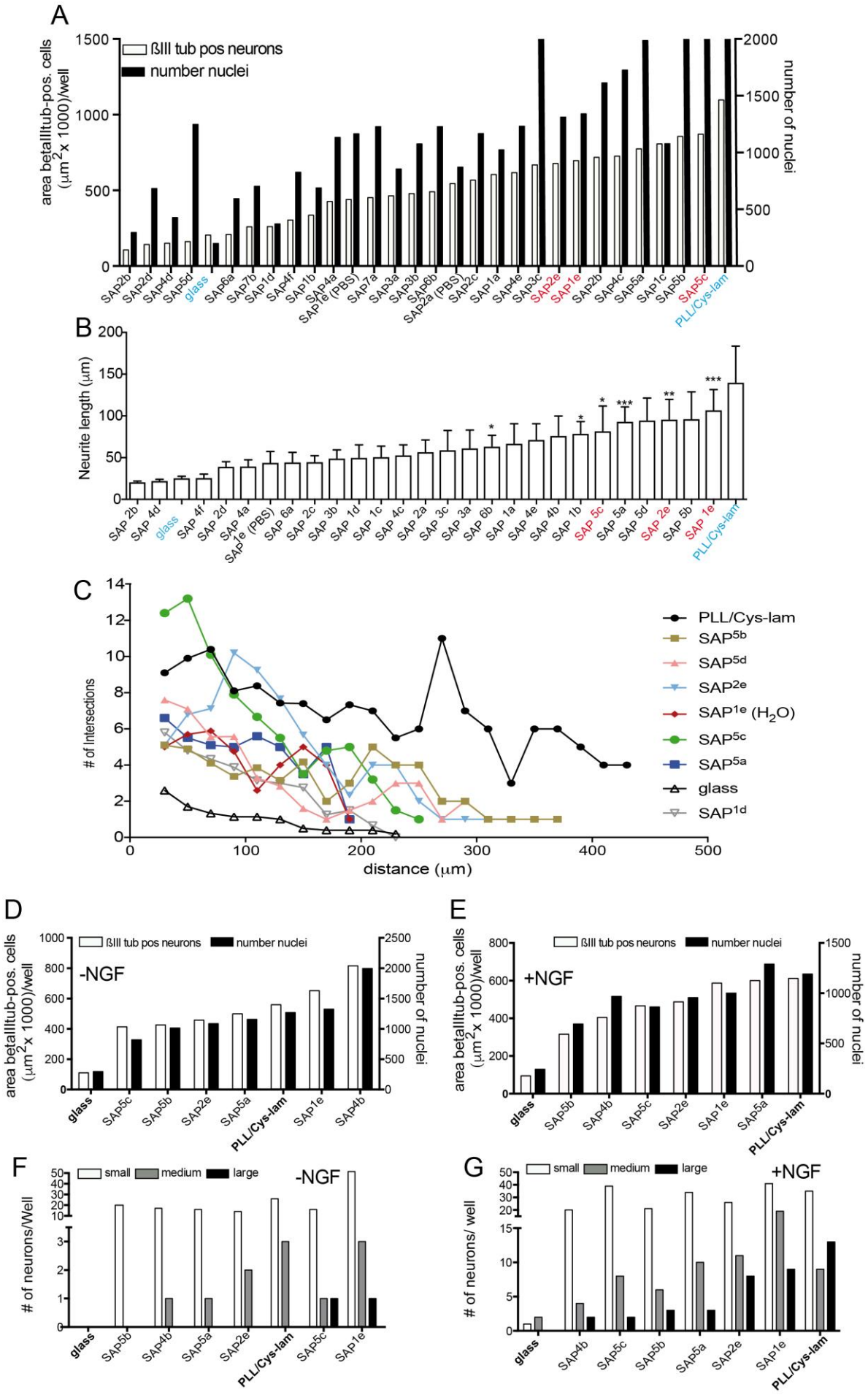
A
ßIII tub pos neurons
number nuclei
area betaIIItub-pos. cells (µm²x 1000)/well
number of nuclei
SAP2b SAP2d SAP4d SAP5d glass SAP6a SAP7b SAP1d SAP4f SAP1b SAP4a SAP1e (PBS) SAP7a SAP3a SAP3b SAP6b SAP2a (PBS) SAP2c SAP1a SAP4e SAP3c SAP2e SAP1e SAP2b SAP4c SAP5a SAP1c SAP5b SAP5c PLL/Cys-lam
B
Neurite length (µm)
SAP 2b SAP 4d glass SAP 4f SAP 2d SAP 4a SAP1e (PBS) SAP 6a SAP 2c SAP 3b SAP 1d SAP 1c SAP 4c SAP 2a SAP 3c SAP 3a SAP 6b SAP 1a SAP 4e SAP 4b SAP 1b SAP 5c SAP 5a SAP 5d SAP 2e SAP 5b SAP 1e PLL/Cys-lam
C
# of Intersections
distance (µm)
PLL/Cys-lam
SAP5b
SAP5d
SAP2e
SAP1e (H2O)
SAP5c
SAP5a
glass
SAP1d
D
-NGF
ßIII tub pos neurons
number nuclei
area betaIIItub-pos. cells (µm²x 1000)/well
number of nuclei
glass SAP5c SAP5b SAP2e SAP5a PLL/Cys-lam SAP1e SAP4b
E
+NGF
ßIII tub pos neurons
number nuclei
area betaIIItub-pos. cells (µm²x 1000)/well
number of nuclei
glass SAP5b SAP4b SAP5c SAP2e SAP1e SAP5a PLL/Cys-lam
F
-NGF
small
medium
large
# of neurons/Well
glass SAP5b SAP4b SAP5a SAP2e PLL/Cys-lam SAP5c SAP1e
G
+NGF
small
medium
large
# of neurons/ well
glass SAP4b SAP5c SAP5b SAP5a SAP2e SAP1e PLL/Cys-lam

Figure S4 (previous page)

Quantification of total cell number and neuronal cells only for SAPs

(A) Quantification of total neuronal area (white bars) and number of neuronal nuclei (black bars) for DRG cell cultures grown on the different SAPs indicated.

(B) Quantification of average neurite length (in μm) of the longest neurite/neuron for all conditions. Data are depicted as mean ± SEM.

(C) Scholl analysis of the number of branches ("intersections") in relation to the distance apart from the cell body. Neurons grown on PLL/Cys-lam had the highest number of branches whereas neurons grown on glass had the fewest branches. Neurons grown on SAP^{5c}, SAP^{1e} and SAP^{2e} also had a high number of branches.

(D, E) Selected SAPs were compared with glass (negative control) and the growth substrate PLL/Cys-laminin as positive control. Total neuronal area (white bars) and number of neuronal nuclei (black bars) were quantified (see A). Cells were either cultured without the growth factor NGF (D) or in its presence (E).

(F, G) Same experiment as in (D, E) but graphs depict quantification of neuronal size in the absence (F) or presence (G) of NGF.

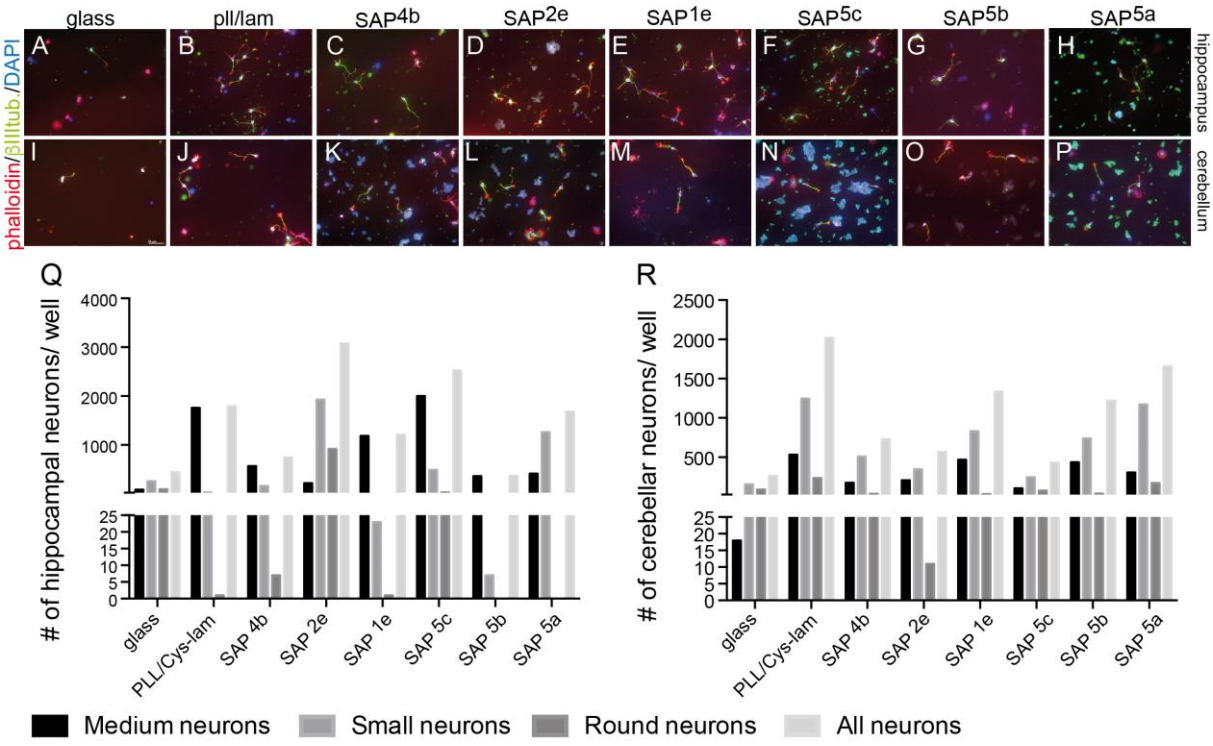

Figure S5

SAPs also stimulate adhesion and neurite growth of primary mouse CNS hippocampal and cerebellar neurons

(A-P) Mouse primary hippocampal (A-H) or cerebellar (I-P) neurons were cultured on the respective SAPs, glass or PLL/Cys-lam. Cells were stained with phalloidin to label F-actin and βIII tubulin to label neurons, respectively. DAPI was used to label nuclei. Please note that some SAPs (SAP^{4b}, SAP^{2e}, SAP^{5c}) were also positively stained for DAPI.

(Q, R) Quantification hippocampal (Q) and cerebellar (R) neuron growth by calculating number of all neurons and neurons with no neurites (”round neurons”) or small and medium size. Scale-bars (A-P) = 50 μm

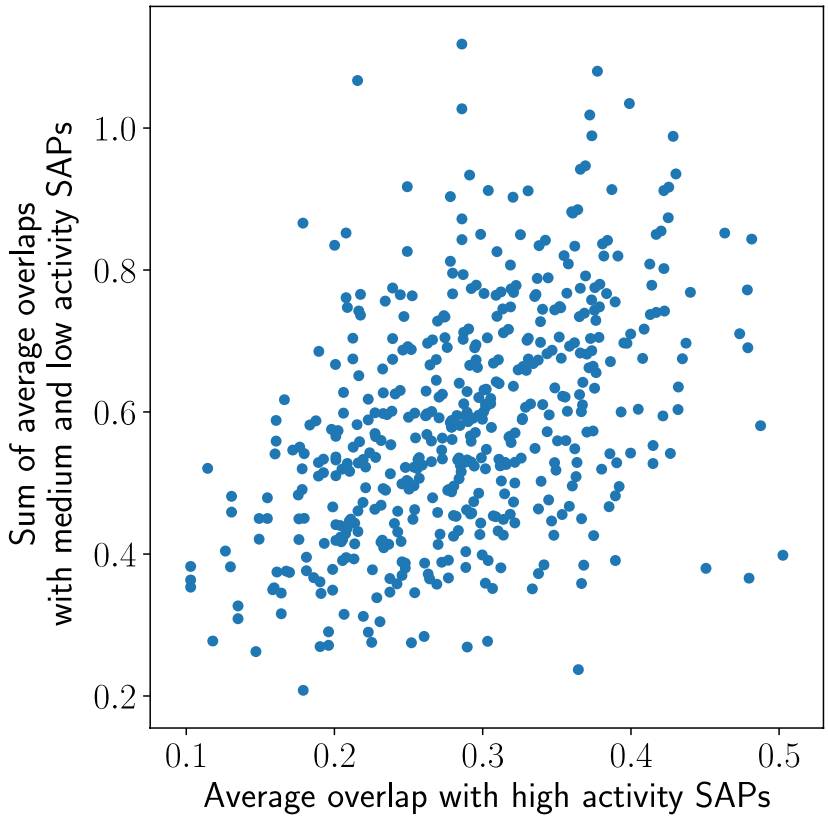

Figure S6

Overlap index I between constructed sequences from library and SAPs. Sequences represented by the points on the lower-right corner have high values of Q and predicted to have higher activity.

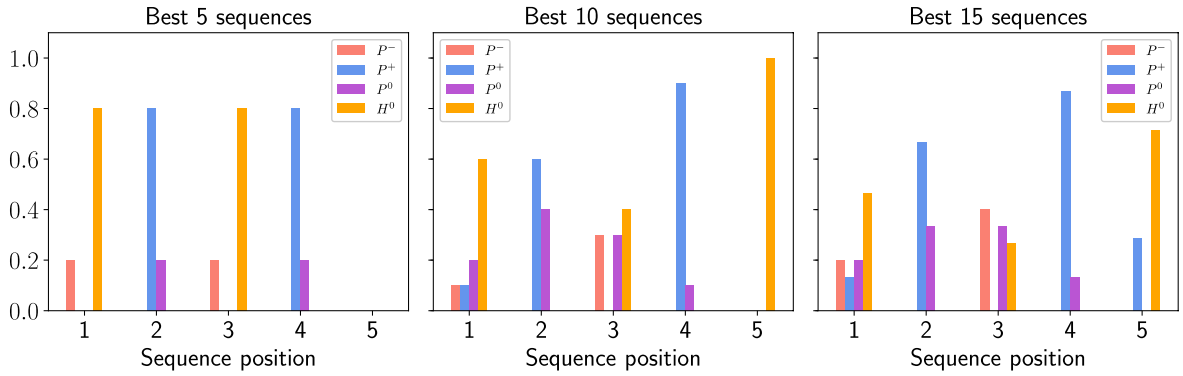

Figure S7

Histogram showing occurrences of amino acid types at different sequence positions. The recurring motif that emerges from the analysis is $H^0P^+H^0P^+H^0$. Note that the third position shows higher variability.

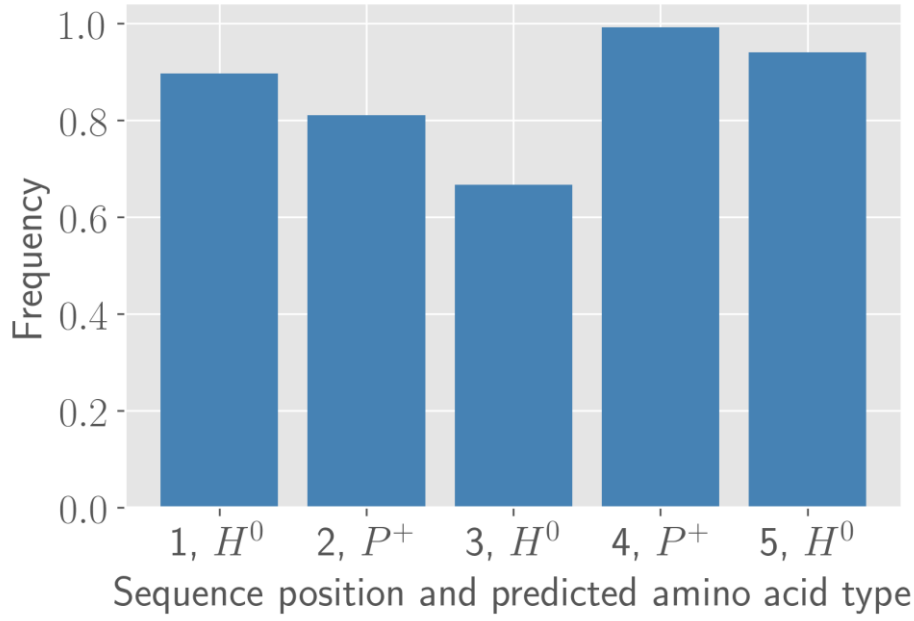

Figure S8

Results from the train-test splitting show that on average the most-occurring pattern found from only using the training sets is the same as the predicted pattern $H^0P^+H^0P^+H^0$ found using the whole dataset. This confirms that our predicted sequence is robust.

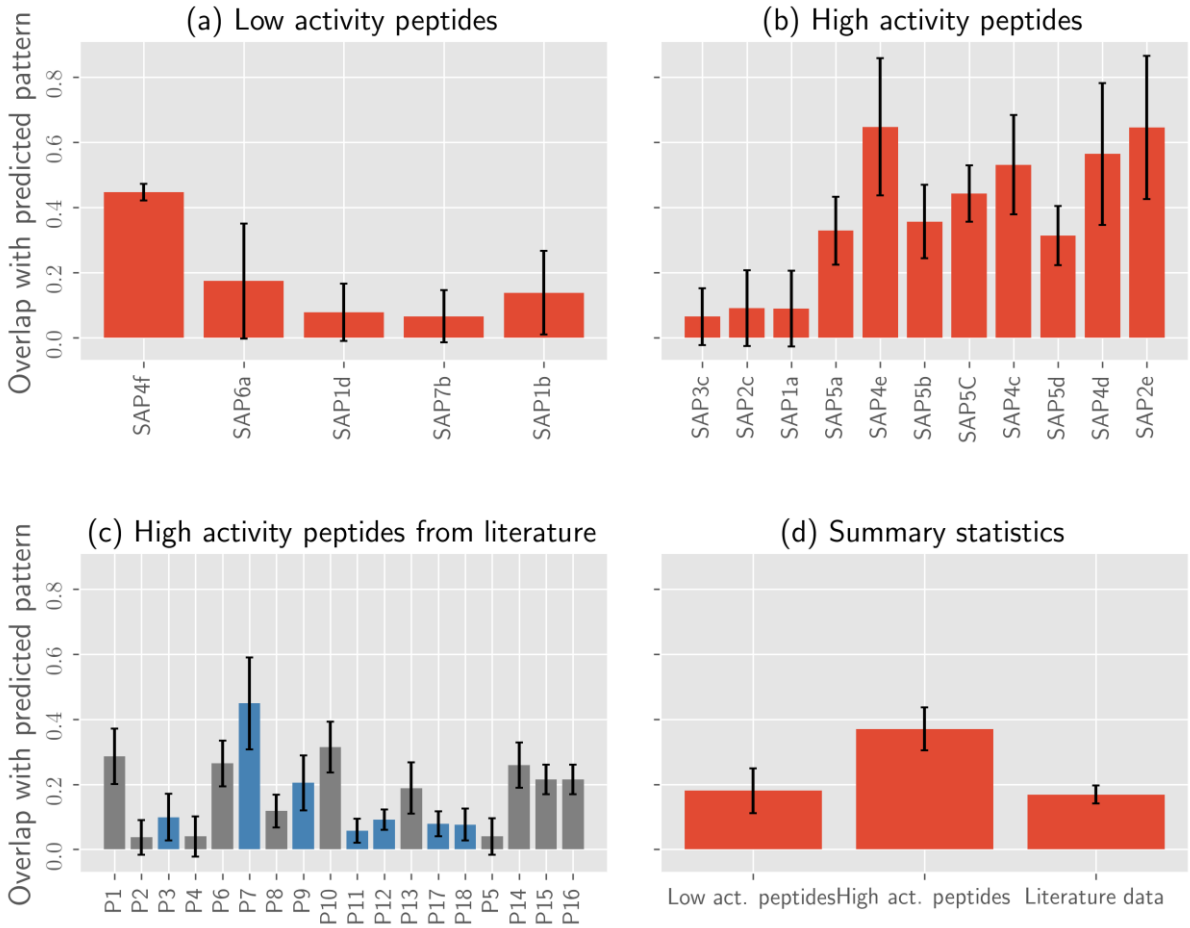

Figure S9

Plot shows the average overlap of the most-occurring pattern found using the training set with: a) Low activity SAPs from our data, b) High activity SAPs from our data, and c) High activity peptides collected from the literature. The peptides drawn with a grey bar in c) denote peptides with net neutral or negative charge and the blue bars denote peptides with net positive charge. Plot d) shows the mean overlap for each of low, high and literature data.

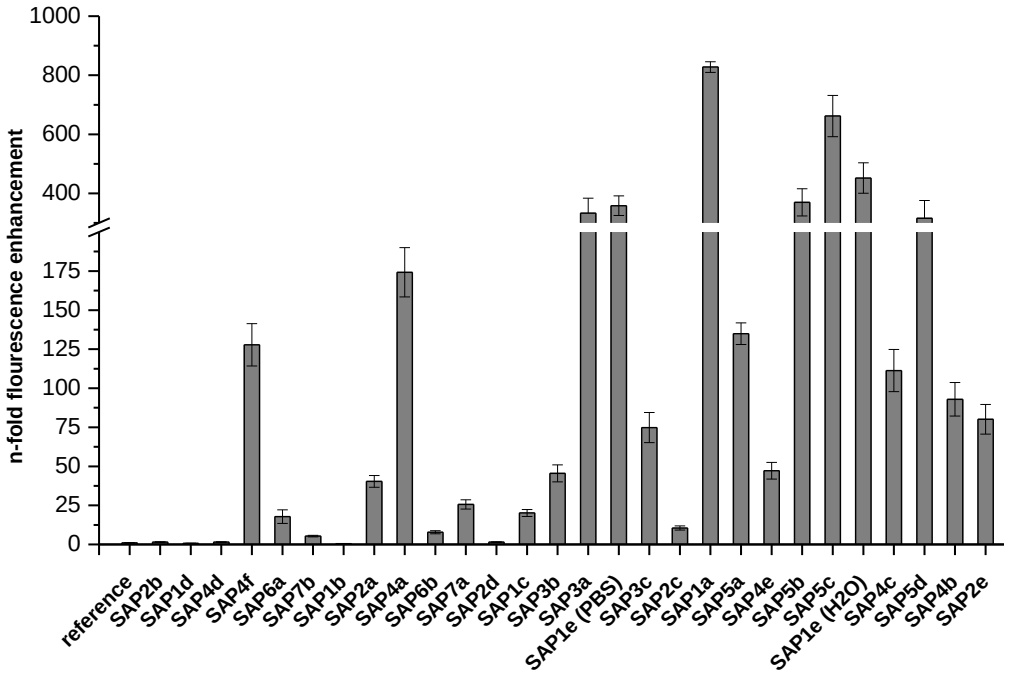

Figure S10

N-fold fluorescence enhancement of preformed fibers (1 day, PBS, 1 mg/mL) with Proteostat®.

SAP^{2b}

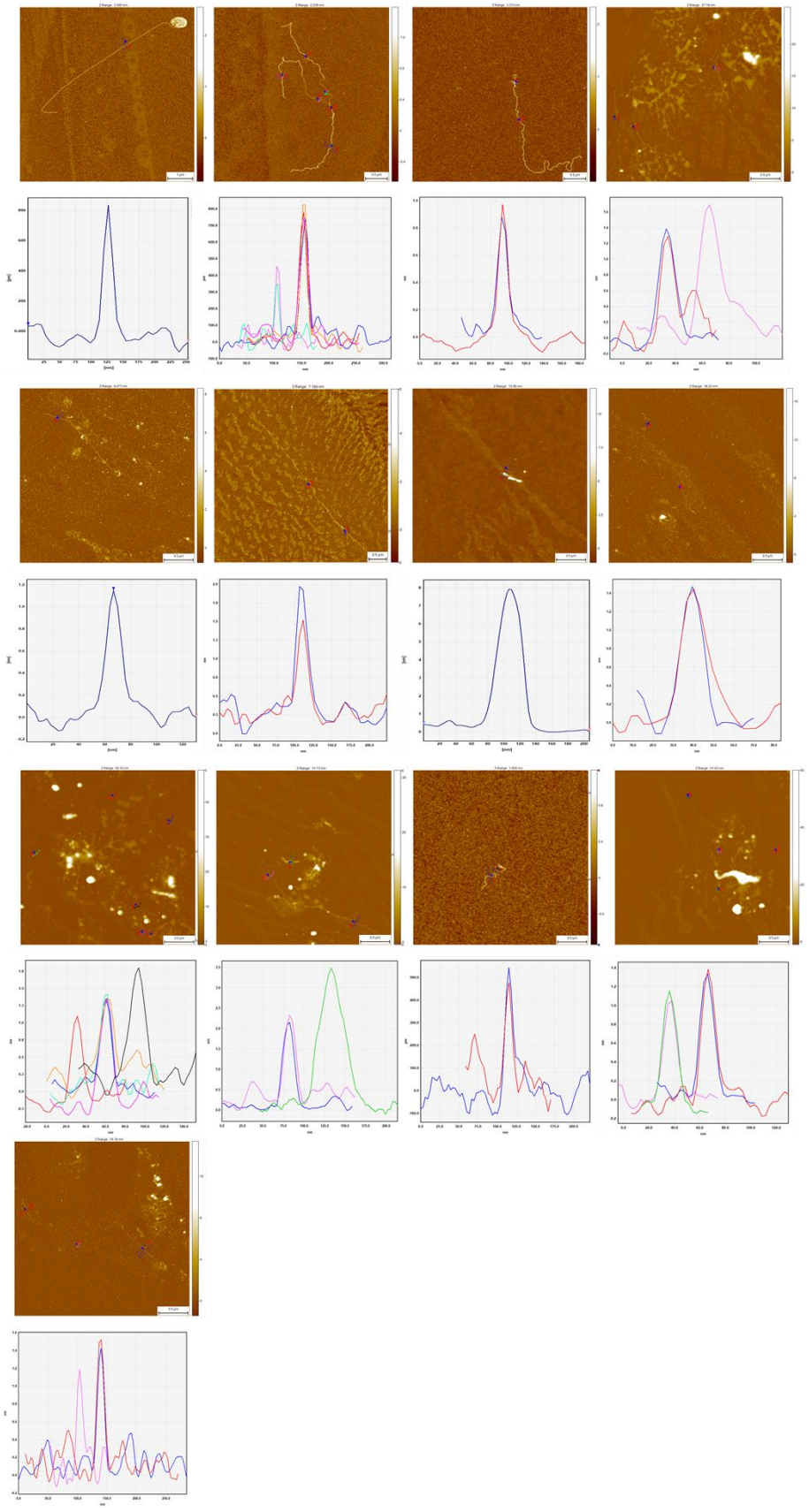

SAP^{2e}

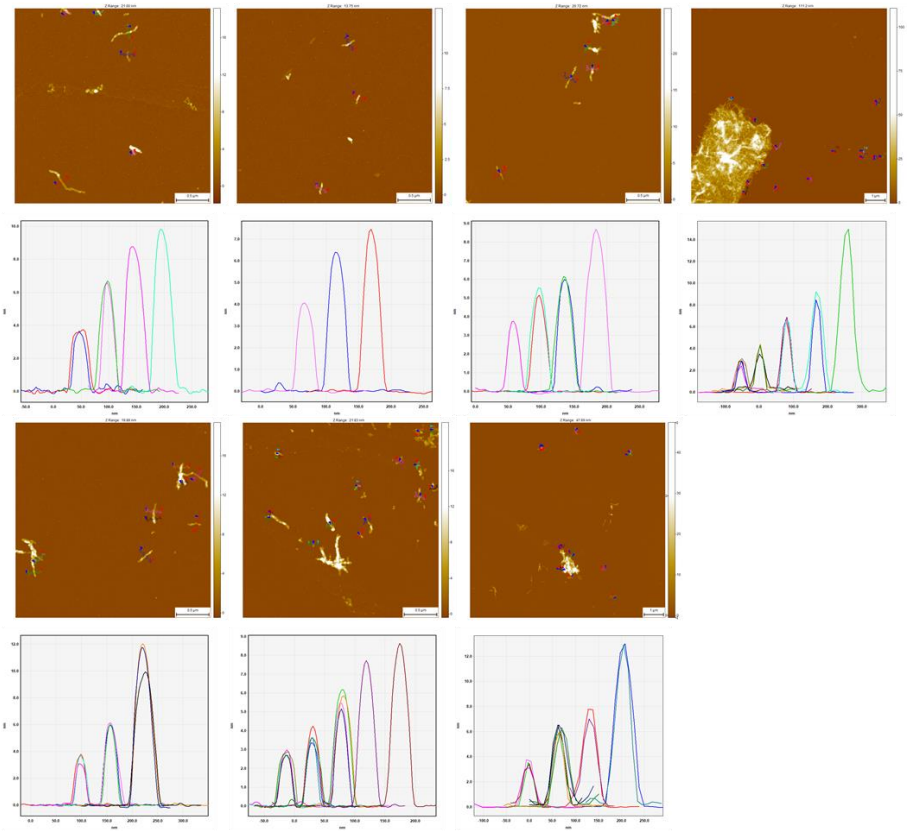

SAP^{5c}

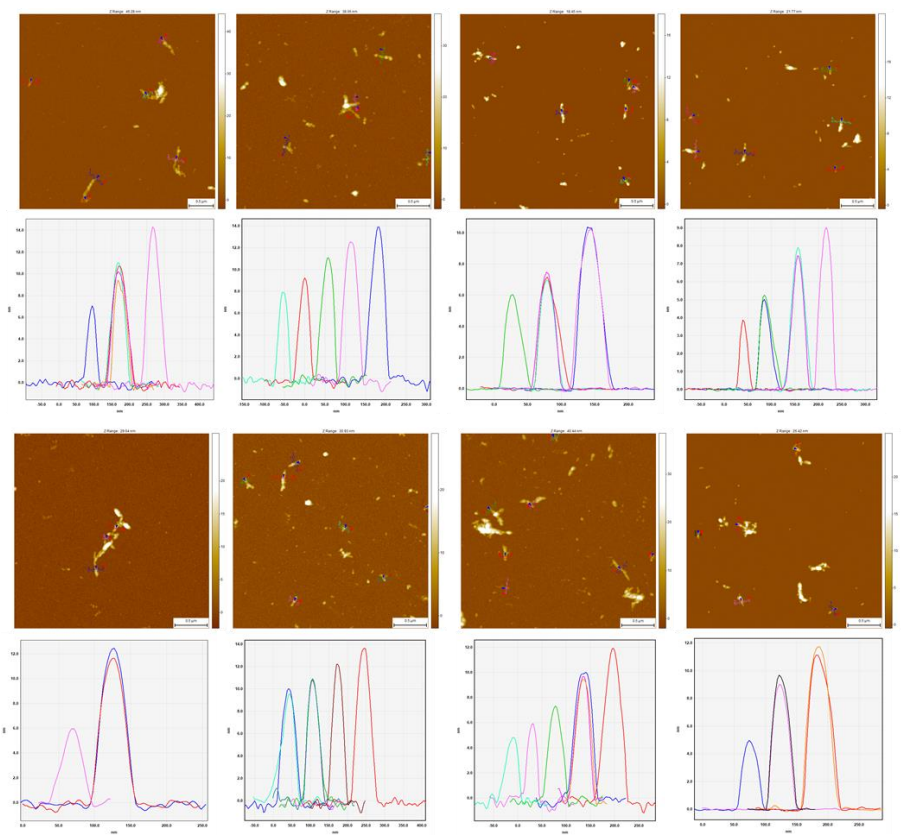

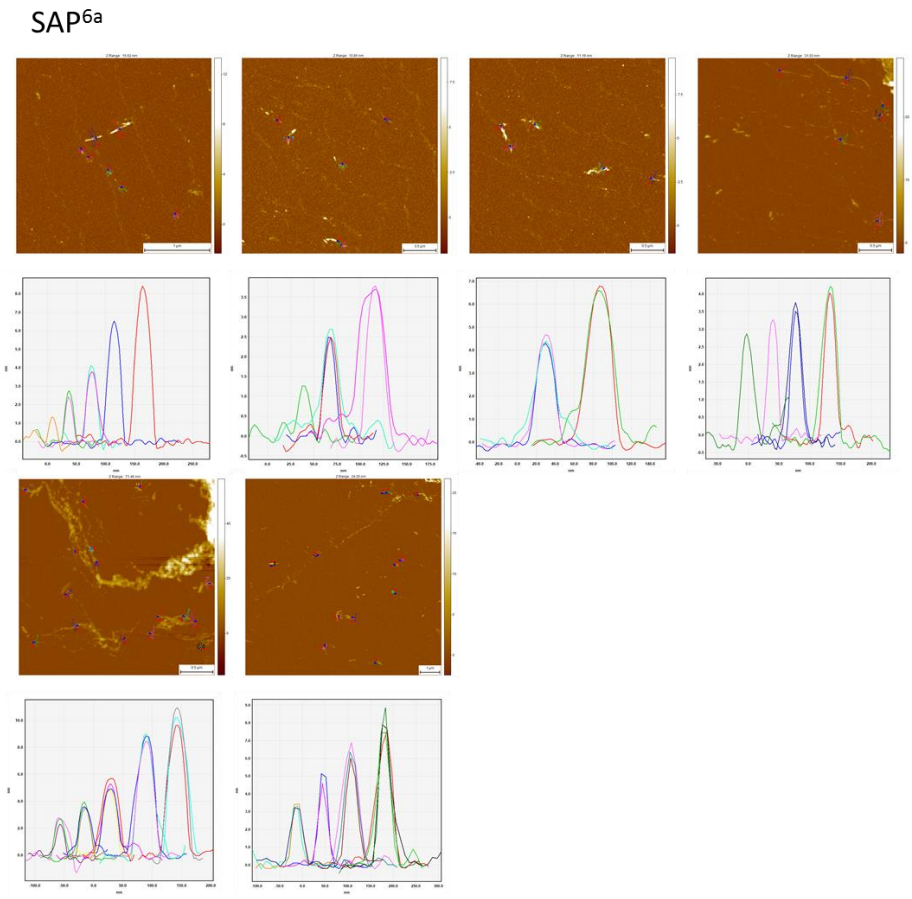

Figure S11

Measurement of cross-sectional height of several fibers in detail for SAP^{2b}, SAP^{2e}, SAP^{5c} and SAP^{6a}.

SAP^{1a}

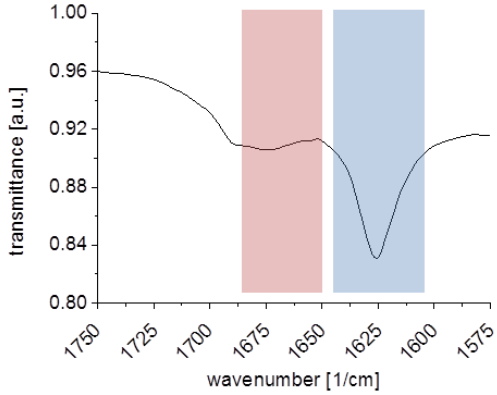

SAP^{1b}

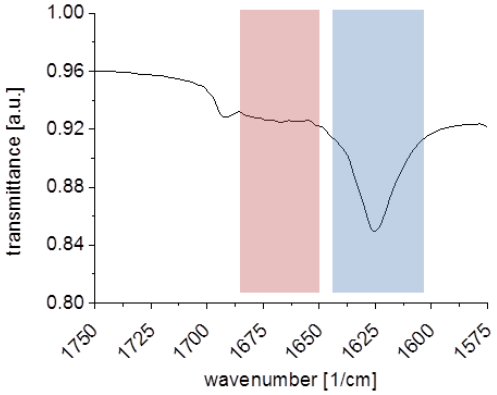

SAP^{1c}

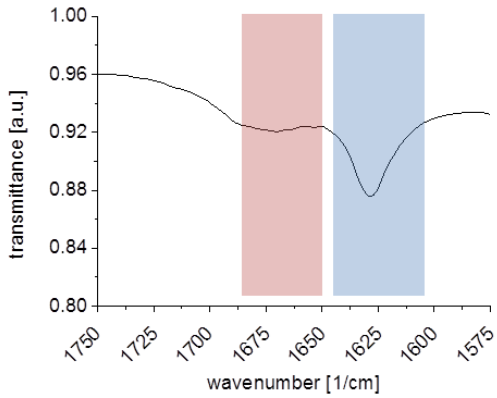

SAP^{1d}

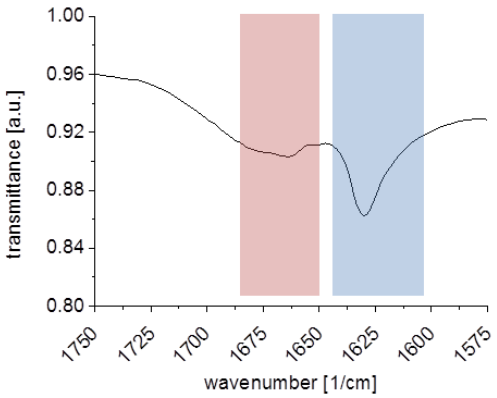

SAP^{1e} (PBS)

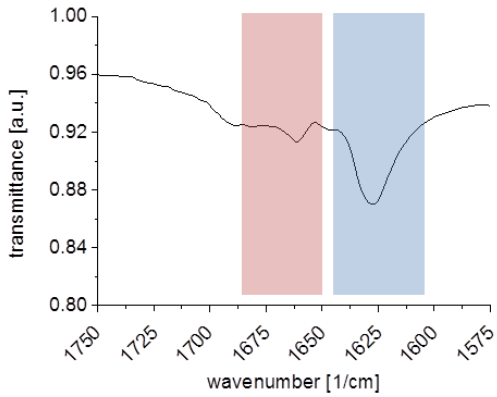

SAP^{1e} (H_2O)

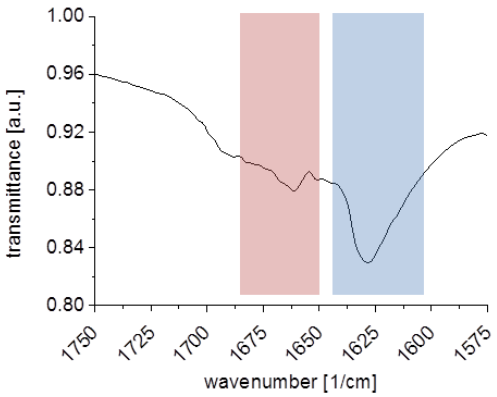

SAP^{2a}

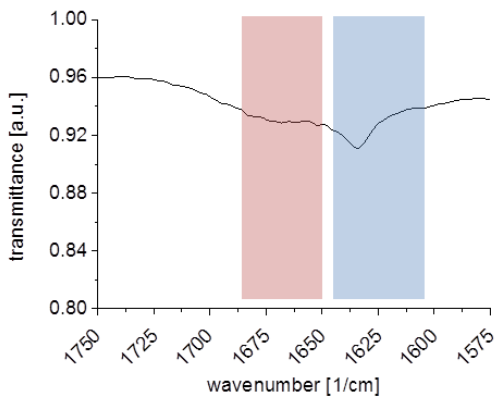

SAP^{2b}

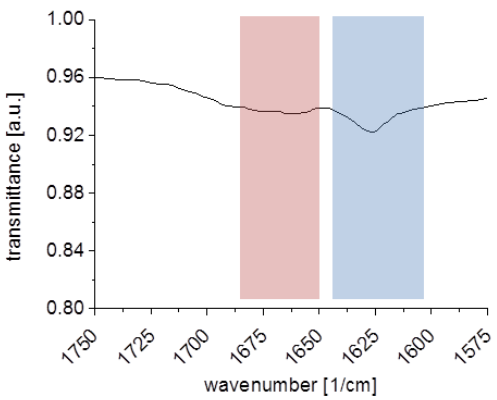

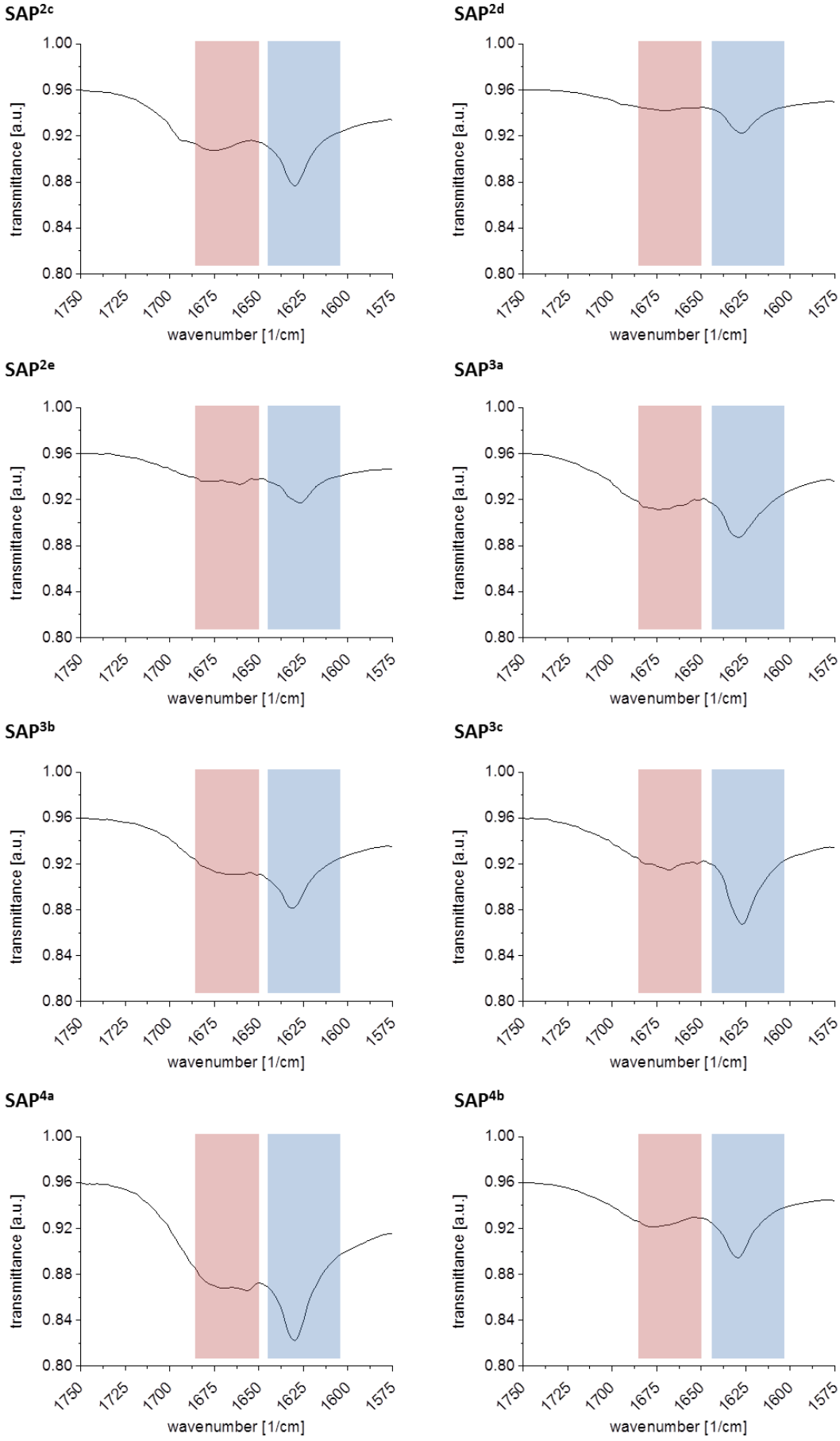
SAP2c
SAP2d
SAP2e
SAP3a
SAP3b
SAP3c
SAP4a
SAP4b
transmittance [a.u.]
1.00
0.96
0.92
0.88
0.84
0.80
1750
1725
1700
1675
1650
1625
1600
1575
wavenumber [1/cm]

SAP^{4c}

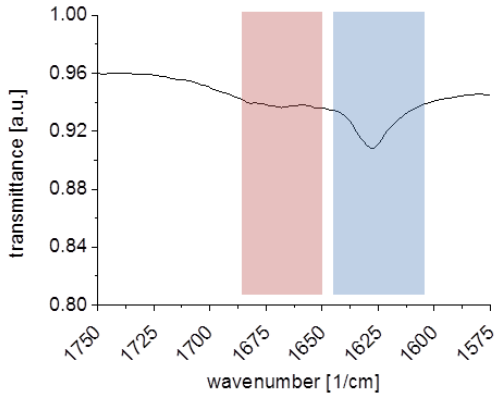

SAP^{4d}

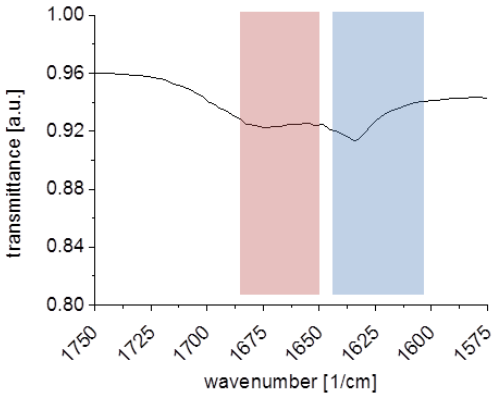

SAP^{4e}

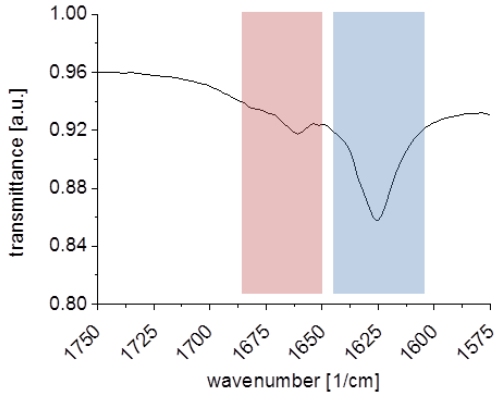

SAP^{4f}

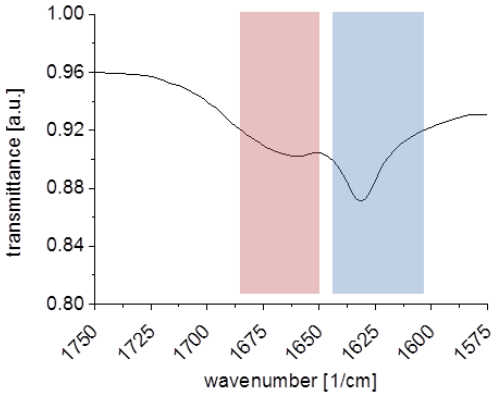

SAP^{5a}

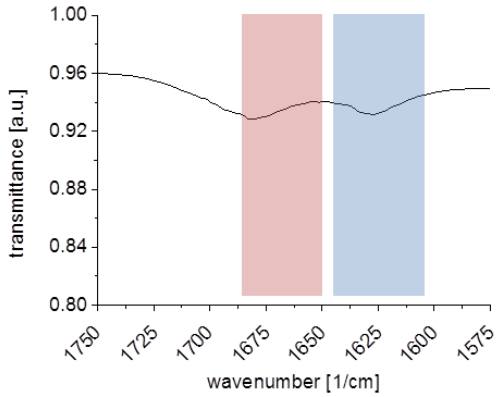

SAP^{5b}

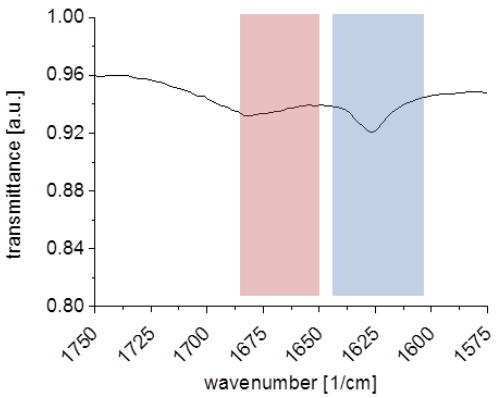

SAP^{5c}

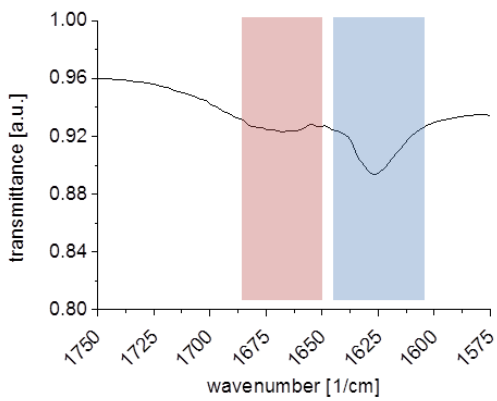

SAP^{5d}

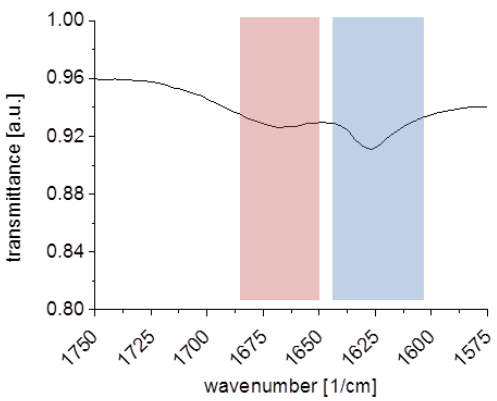

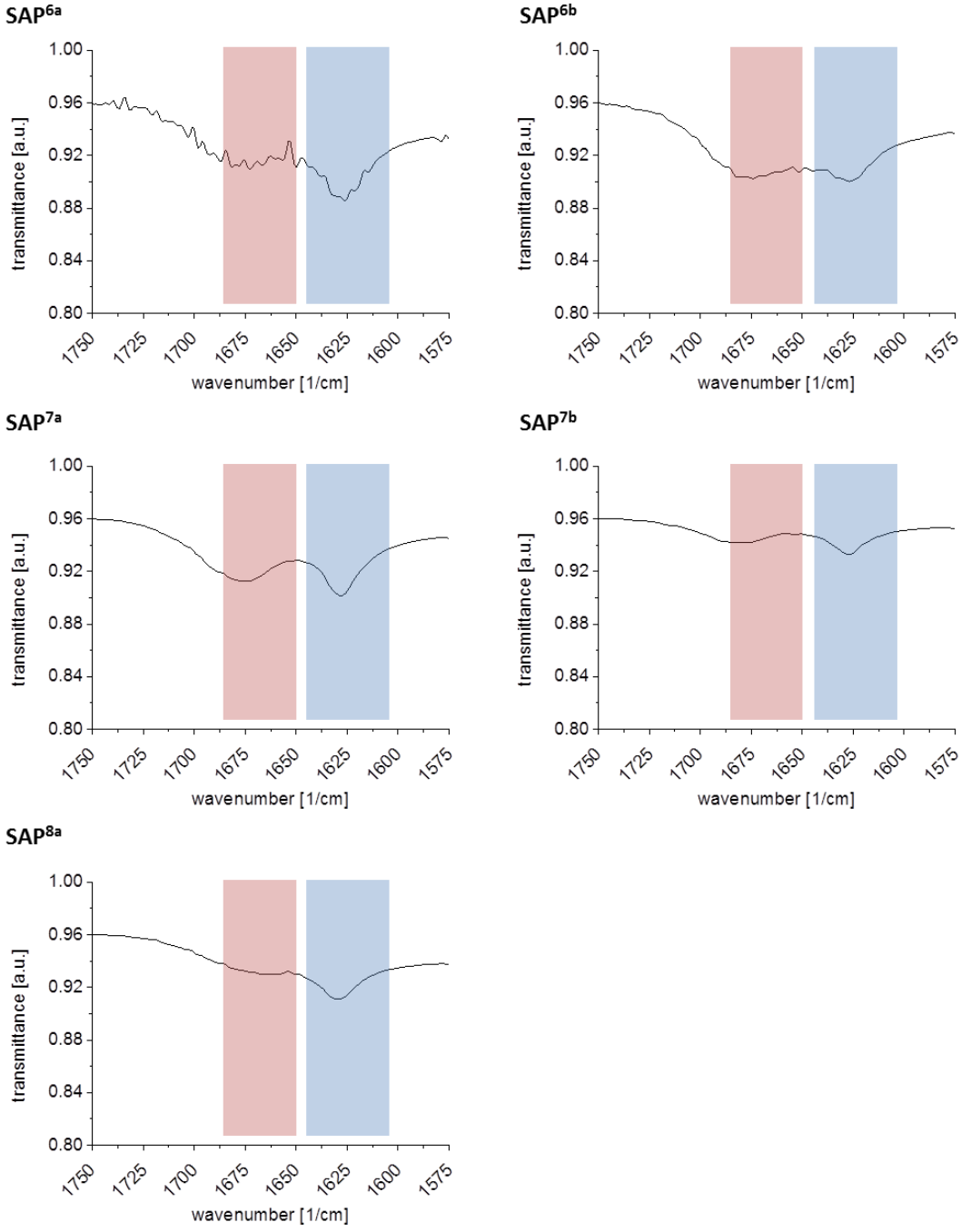

Figure S12

FTIR of all peptides after 1 day incubation in PBS (or ddH_2O) in the amide I region for secondary structure analysis. The blue color represents intermolecular parallel β-sheet peak area and the red color represents α-helix + β-turn peak area.

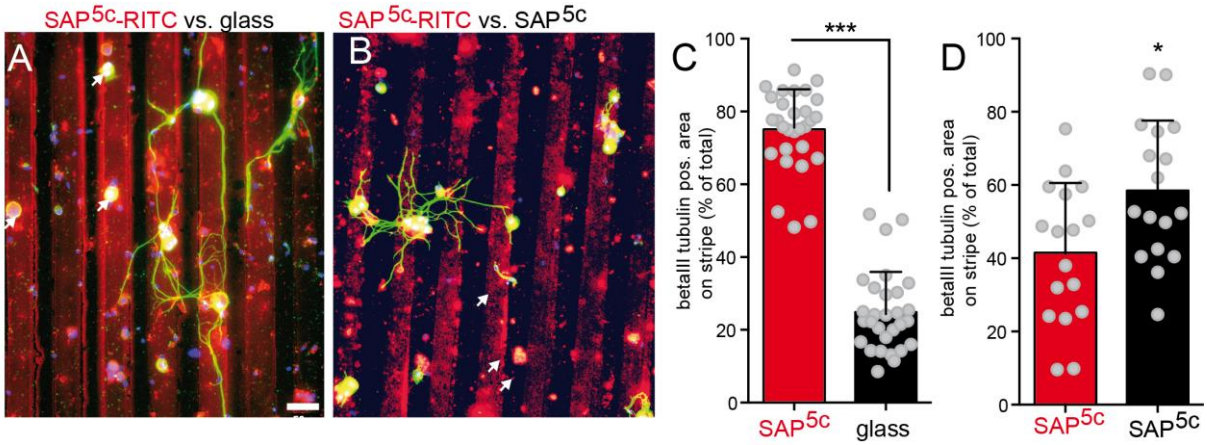

Figure S13

Neurons adhere to SAP5c containing substrates in the stripe assay

(A) Stripe assay with alternating lanes consisting of SAP^{5c}-RITC (red lanes) and glass only (dark lanes). DRG neuronal cell bodies (arrows) and outgrowing neurites preferred to grow on SAP^{5c}.

(B) Stripe assay with both lanes consisting of SAP^{5c}. Here, random outgrowth and localization of neuronal structures was observed.

(C) Quantification of experiments consisting of SAP^{5c}-positive stripes vs. glass only stripes. The majority of neurons was localized on SAP5c. Each dot represents one picture taken from independent stripe assays.

(D) Quantification of stripe assays with both lanes containing SAP^{5c}. Here, neurons grew almost equally well on both stripes. Each dot represents one picture taken from independent stripe assays.

Scale-bar (A, B) = 50 µm

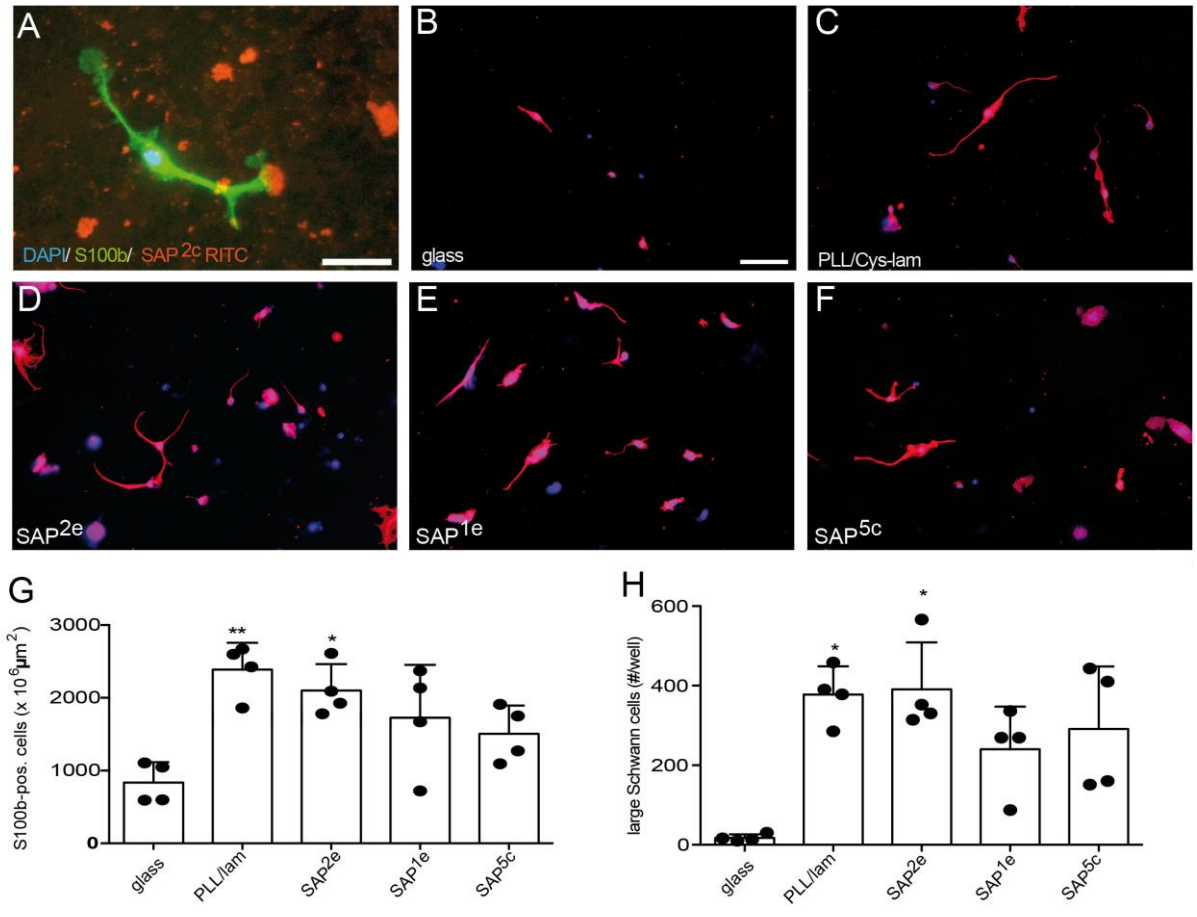

Figure S14

Schwann cell adhesion and growth is enhanced on SAP nanofibers

(A) Mouse Schwann cell stained with S100b (in green) contacts SAP positive plaques (SAP^{2e} conjugated with RITC; in red). DAPI labels the cell nucleus.

(B-F) Glass coverslips were left uncoated (B) or were coated with PLL/Cys-lam (C), SAP^{2e} (D), SAP^{1e} (E) or SAP^{5c} (F). Schwann cells (stained for S100b in red) did not adhere on glass (B) but grew on all three SAPs (D-F) equally well as on PLL/Cys-lam (C). Blue signals are DAPI-positive cell nuclei.

(G, H) Quantification of adhesion (G) and size (H) of Schwann cells on the different substrates. Each circle represents one culture derived from one mouse. Statistical significance was calculated in relation to glass.

Scale-bar (A) = 25 μm; (B-F) = 50 μm

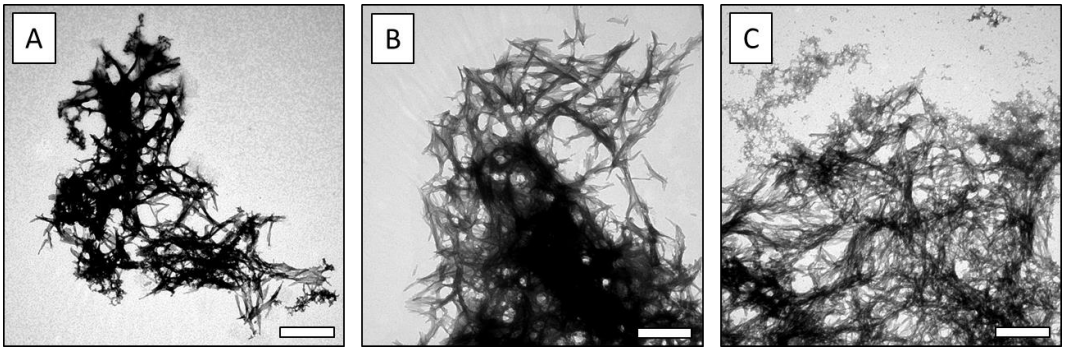

Figure S15

(A) SAP^{5c} fibrils after 1 day incubation in PBS at a final incubation concentration of 1 mg/mL, (B) after 3 more days at 37 °C and (C) after 3 more days in presence of proteinase K (fibril:proteinase K = 20:1 w%) at 37 °C. Scale-bar = 500 nm.

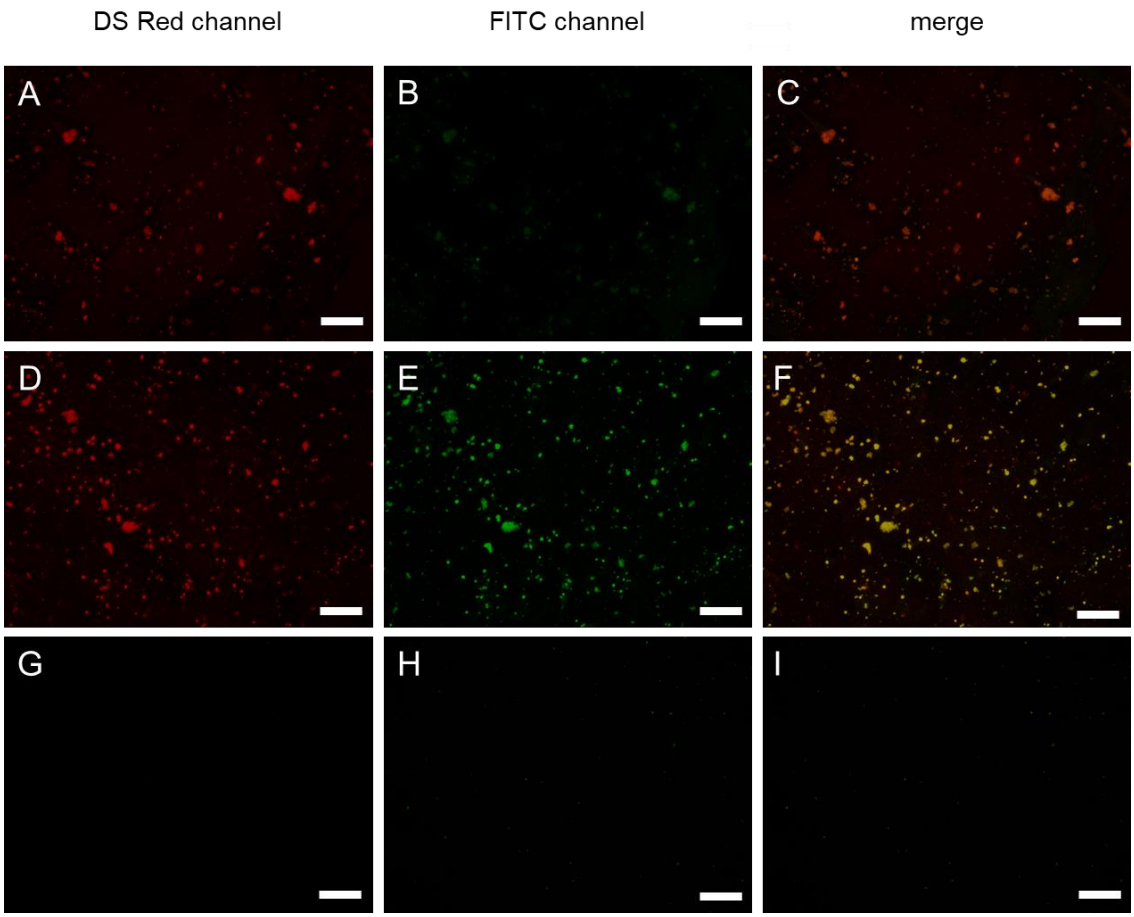

Figure S16

(A-C) Glass coverslips coated with SAP^{5c}-RITC fibrils (fluorescence visible in DS Red channel).

(D-F) Glass coverslips coated with SAP^{5c}-RITC fibrils and incubated with fluorescein labelled human serum album (HSA, fluorescence visible in FITC channel) indicating HSA attachment to SAP^{5c}-RITC fibrils.

(G-I) Glass coverslips were uncoated and incubated with fluorescein labelled HSA.

Scale-bar = 100 µm.

Supporting references

Angeloni, N.L., Bond, C.W., Tang, Y., Harrington, D.A., Zhang, S.M., Stupp, S.I., Mckenna, K.E., and Podlasek, C.A. (2011). Regeneration of the cavernous nerve by Sonic hedgehog using aligned peptide amphiphile nanofibers. *Biomaterials* 32**,** 1091-1101.

Berns, E.J., Alvarez, Z., Goldberger, J.E., Boekhoven, J., Kessler, J.A., Kuhn, H.G., and Stupp, S.I. (2016). A tenascin-C mimetic peptide amphiphile nanofiber gel promotes neurite outgrowth and cell migration of neurosphere-derived cells. *Acta Biomaterialia* 37**,** 50-58.

Berns, E.J., Sur, S., Pan, L., Goldberger, J.E., Suresh, S., Zhang, S., Kessler, J.A., and Stupp, S.I. (2014). Aligned neurite outgrowth and directed cell migration in self-assembled monodomain gels. *Biomaterials* 35**,** 185-195.

Choe, S., Bond, C.W., Harrington, D.A., Stupp, S.I., Mcvary, K.T., and Podlasek, C.A. (2017). Peptide amphiphile nanofiber hydrogel delivery of sonic hedgehog protein to the cavernous nerve to promote regeneration and prevent erectile dysfunction. *Nanomedicine-Nanotechnology Biology and Medicine* 13**,** 95-101.

Ellis-Behnke, R.G., Liang, Y.X., You, S.W., Tay, D.K.C., Zhang, S.G., So, K.F., and Schneider, G.E. (2006). Nano neuro knitting: Peptide nanofiber scaffold for brain repair and axon regeneration with functional return of vision. *Proceedings of the National Academy of Sciences of the United States of America* 103**,** 5054-5059.

Ferreira TA, Blackman AV, Oyrer J, Jayabal S, Chung AJ, Watt AJ, Sjostrom PJ, van Meyel DJ (2014) Neuronal morphometry directly from bitmap images. Nature methods 11:982-984.

Francis, N.L., Bennett, N.K., Halikere, A., Pang, Z.P.P., and Moghe, P.V. (2016). Self-Assembling Peptide Nanofiber Scaffolds for 3-D Reprogramming and Transplantation of Human Pluripotent Stem Cell-Derived Neurons. *Acs Biomaterials Science & Engineering* 2**,** 1030-1038.

Greene, J.J., Mcclendon, M.T., Stephanopoulos, N., Alvarez, Z., Stupp, S.I., and Richter, C.P. (2018). Electrophysiological assessment of a peptide amphiphile nanofiber nerve graft for facial nerve repair. *Journal of Tissue Engineering and Regenerative Medicine* 12**,** 1389-1401.

Knoll, B., Weinl, C., Nordheim, A., and Bonhoeffer, F. (2007). Stripe assay to examine axonal guidance and cell migration. *Nat Protoc* 2(5)**,** 1216-1224.

Kim, J.H., Jung, Y., Kim, B.S., and Kim, S.H. (2013). Stem cell recruitment and angiogenesis of neuropeptide substance P coupled with self-assembling peptide nanofiber in a mouse hind limb ischemia model. *Biomaterials* 34**,** 1657-1668.

Kyte, J., and Doolittle, R.F. (1982). A simple method for displaying the hydropathic character of a protein. *J Mol Biol* 157(1)**,** 105-132.

Li, X., Liu, X., Josey, B., Chou, C.J., Tan, Y., Zhang, N., and Wen, X. (2014). Short Laminin Peptide for Improved Neural Stem Cell Growth. *STEM CELLS Translational Medicine* 3**,** 662-670.

Liang, P., Xiong, J.S., Zhao, L.W., Xu, Y., Zhao, J.X., and Liu, Q. (2015). Recombinant self-assembling 16-residue peptide nanofiber scaffolds for neuronal axonal outgrowth. *Engineering in Life Sciences* 15**,** 152-158.

Liu, Y., Ye, H., Satkunendrarajah, K., Yao, G.S., Bayon, Y., and Fehlings, M.G. (2013). A self-assembling peptide reduces glial scarring, attenuates post-traumatic inflammation and promotes neurological recovery following spinal cord injury. *Acta biomaterialia* 9**,** 8075-8088.

Lu, C., Wang, Y., Yang, S., Wang, C., Sun, X., Lu, J., Yin, H., Jiang, W., Meng, H., Rao, F., Wang, X., and Peng, J. (2018). Bioactive Self-Assembling Peptide Hydrogels Functionalized with Brain-Derived Neurotrophic Factor and Nerve Growth Factor Mimicking Peptides Synergistically Promote Peripheral Nerve Regeneration. *ACS Biomaterials Science & Engineering* 4**,** 2994-3005.

Pedregosa, F., Varoquaux, G., Gramfort, A., Michel, V., Thirion, B., Grisel, O., Blondel, M., Prettenhofer, P., Weiss, R., Dubourg, V., Vanderplas, J., Passos, A., Cournapeau, D., Brucher, M., Perrot, M., and Duchesnay, E. (2011). Scikit-learn: Machine Learning in Python. *Journal of Machine Learning Research* 12**,** 2825-2830.

Shi, W., Huang, C.J., Xu, X.D., Jin, G.H., Huang, R.Q., Huang, J.F., Chen, Y.N., Ju, S.Q., Wang, Y., Shi, Y.W., Qin, J.B., Zhang, Y.Q., Liu, Q.Q., Wang, X.B., Zhang, X.H., and Chen, J. (2016). Transplantation of RADA16-BDNF peptide scaffold with human umbilical cord mesenchymal stem cells forced with CXCR4 and activated astrocytes for repair of traumatic brain injury. *Acta Biomaterialia* 45**,** 247-261.

Tavakol, S., Mousavi, S.M.M., Tavakol, B., Hoveizi, E., Ai, J., and Sorkhabadi, S.M.R. (2017). Mechano-Transduction Signals Derived from Self-Assembling Peptide Nanofibers Containing Long Motif of Laminin Influence Neurogenesis in In-Vitro and In-Vivo. *Molecular Neurobiology* 54**,** 2483-2496.

Tavakol, S., Saber, R., Hoveizi, E., Tavakol, B., Aligholi, H., Ai, J., and Rezayat, S.M. (2016). Self-Assembling Peptide Nanofiber Containing Long Motif of Laminin Induces Neural Differentiation, Tubulin Polymerization, and Neurogenesis: In Vitro, Ex Vivo, and In Vivo Studies. *Molecular Neurobiology* 53**,** 5288-5299.

Walther, P., Wang, L., Liessem, S., and Frascaroli, G. (2010). Viral infection of cells in culture--approaches for electron microscopy. *Methods Cell Biol* 96**,** 603-618. doi: 10.1016/S0091-679X(10)96025-1.

Yamagishi S, Hampel F, Hata K, Del Toro D, Schwark M, Kvachnina E, Bastmeyer M, Yamashita T, Tarabykin V, Klein R, Egea J (2011) FLRT2 and FLRT3 act as repulsive guidance cues for Unc5-positive neurons. The EMBO journal 30:2920-2933.

Zou, Z., Zheng, Q., Wu, Y., Song, Y., and Wu, B. (2009). Growth of rat dorsal root ganglion neurons on a novel self-assembling scaffold containing IKVAV sequence. *Materials Science and Engineering: C* 29**,** 2099-2103.